TRANSFORMATION TOUGHENING OF CERAMICS(U) ROCKWELL
INTERNATIONAL THOUSAND OAKS CA SCIENCE CENTER
D B MARSHALL OCT 87 SC5444 AR AFOSR-TR-87-1854

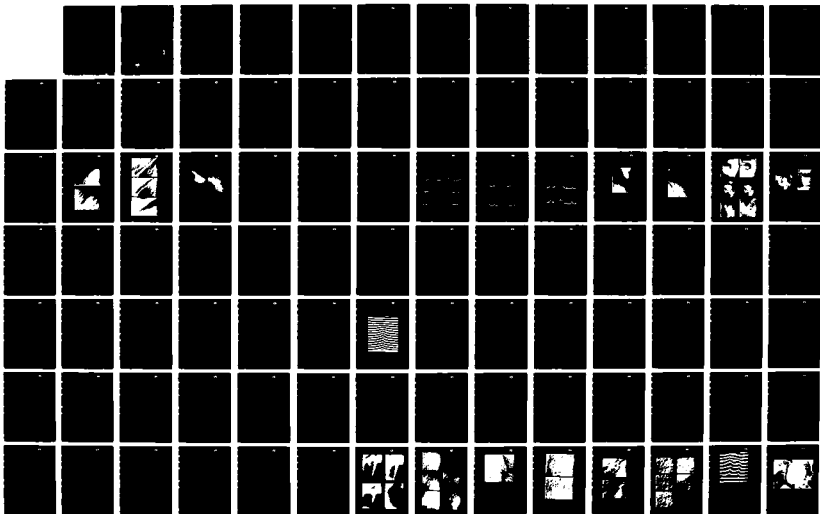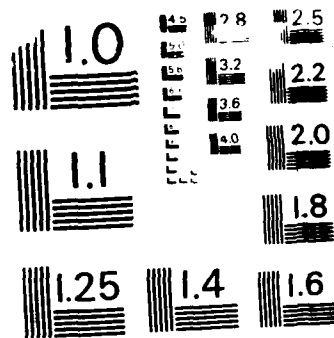MICROCOPY RESOLUTION TEST CHART

NATIONAL BUREAU OF STANDARDS-1963-

SC5444.AR

Copy No. 2

TRANSFORMATION TOUGHENING OF CERAMICS

ANNUAL REPORT NO. 2 FOR THE PERIOD
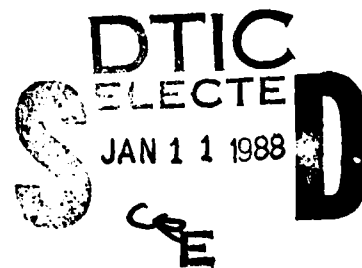September 1, 1986 through August 31, 1987

CONTRACT NO. F49620-85-C-0143
PROJECT NO. 2306/A2

Prepared for

Air Force Office of Scientific Research
Directorate of Electronic & Material Sciences
Building 410
Bolling AFB, DC 20332-6448

D.B. Marshall
Principal Investigator

DTIC
ELECTE
JAN 1 1 1988

OCTOBER 1987

Rockwell International
Science Center

REPORT DOCUMENTATION PAGE

1a. REPORT SECURITY CLASSIFICATION	1b. RESTRICTIVE MARKINGS
UNCLASSIFIED	

2a. SECURITY CLASSIFICATION AUTHORITY	3. DISTRIBUTION/AVAILABILITY OF REPORT
	Approved for public release; distribution unlimited
2b. CLASSIFICATION/DOWNGRADING SCHEDULE	

4. PERFORMING ORGANIZATION REPORT NUMBER(S)	5. MONITORING ORGANIZATION REPORT NUMBER(S)
SC5444.AR	**AFOSR-TR. 87-1854**

6a. NAME OF PERFORMING ORGANIZATION	6b. OFFICE SYMBOL (If Applicable)	7a. NAME OF MONITORING ORGANIZATION
ROCKWELL INTERNATIONAL Science Center		AFOSR

6c. ADDRESS (City, State, and ZIP Code)	7b. ADDRESS (City, State and ZIP Code)
1049 Camino Dos Rios **Thousand Oaks, CA 91360**	Blg 410 BAFB DC. 20332-6448

8a. NAME OF FUNDING/SPONSORING ORGANIZATION	8b. OFFICE SYMBOL (If Applicable)	9. PROCUREMENT INSTRUMENT IDENTIFICATION NUMBER
Air Force Office of Scientific Research Directorate of Electronic & Material Sciences	NE	**CONTRACT NO. F49620-85-C-0143**

8c. ADDRESS (City, State and ZIP Code)	10. SOURCE OF FUNDING NOS.			
Building 410 **Bolling AFB, DC 20332-6448**	PROGRAM ELEMENT NO	PROJECT NO.	TASK NO	WORK UNIT NO
	61102F	23061/ ~A2~	A2	

11. TITLE (Include Security Classification)
TRANSFORMATION TOUGHENING OF CERAMICS

12. PERSONAL AUTHOR(S)
Marshall, D.B.

13a. TYPE OF REPORT	13b. TIME COVERED	14. DATE OF REPORT (Yr., Mo., Day)	15. PAGE COUNT
Annual Report No. 2	FROM **09/01/86** TO **08/31/87**	**1987, OCTOBER**	**116**

16. SUPPLEMENTARY NOTATION

17.	COSATI CODES		18. SUBJECT TERMS (Continue on reverse if necessary and identify by block number)
FIELD	GROUP	SUB. GR.	

19. ABSTRACT (Continue on reverse if necessary and identify by block number)

The mechanical properties of high toughness magnesia-partially stabilized zirconia were found to be severely degraded by a single cooling cycle between room temperature and −196°C. In-situ Raman spectroscopy and optical interference measurements, and room temperature x-ray diffraction were used to correlate the changes in mechanical properties with structural changes; cooling to temperatures below ~−100°C caused transformation of most of the tetragonal precipitates that are responsible for toughening to a new phase with unit cell volume intermediate between those of the tetragonal and monoclinic phases. The new phase was stable with heating to 300°C, but at 400°C it transformed back to the tetragonal structure. After heating to 400°C the original high-toughness mechanical properties were also restored.

A new approach for measuring the nature and distribution of strains within transformation zones surrounding cracks in transformation toughened materials was demonstrated, using Mg-PSZ. The method involves measuring out-of-plane distortions adjacent to a surface-breaking crack and comparing the measurements with computed displacements. The fraction of transformation was found to be a strongly varying function of distance from the crack plane. Over most of the transformation zone the transformation strains were dilational (i.e., shear strains relieved by twinning),

20. DISTRIBUTION/AVAILABILITY OF ABSTRACT	21. ABSTRACT SECURITY CLASSIFICATION
UNCLASSIFIED/UNLIMITED ☐ SAME AS RPT. ☒ DTIC USERS ☐	**UNCLASSIFIED**

| 22a. NAME OF RESPONSIBLE INDIVIDUAL	22b. TELEPHONE NUMBER (Include Area Code)	22c. OFFICE SYMBOL
Dr. Wittman	202-767-4984	NE

but there was evidence for significant net shear strain persisting near the crack surface. These results have important implications for calculating the degree of transformation toughening. Factors that influence nucleation, reversibility, and stabilization of transformation in various ZrO_2 containing ceramics were examined. Direct observations of reversible and irreversible transformation were presented and the thermodynamics of the transformation were discussed with special reference to the influence of particle aspect ratio on stability of the transformation.

Mechanisms of grain growth control (critical for fabricating transformation toughened ceramics) in the two-phase region of the ZrO_2/Y_2O_3 system were investigated by measuring phase partitioning and microstructural development during sintering of a metastable precursor with a very uniform initial distribution of Y_2O_3 additive. Phase partitioning began with small compositional fluctuations between grains rather than by nucleation of grains with two equilibrium compositions, and the partitioning was extremely sluggish at normal sintering temperatures. Grain growth was extremely slow during the early stages of partitioning, leading to the hypothesis that strain energy due to lattice parameter mismatch inhibits grain boundary movement and hence grain growth.

TABLE OF CONTENTS
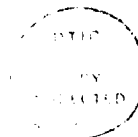
1.0 INTRODUCTION

The goal of this research is to develop a basic scientific understanding of the factors that dictate microstructural evolution and mechanical properties of transformation-toughened ceramics, in order to enable development of new transformation-toughened materials with higher temperature capabilities than existing systems. The work has focused on two main topics. One is the understanding of transformation mechanisms and relations between the microstructural characteristics and macroscopic mechanical properties such as strength and toughness. This involves micromechanics modelling based on in situ observations of damage development mechanisms and toughening mechanisms. The other is the control of microstructure during sintering, especially involving the role of second phases and phase partitioning in controlling grain growth. Detailed results of the research done during the past year are contained in four papers that are included as Sections 2 to 5 of this report, and which will be submitted to, or have been published in, the journals or books noted on the title pages. The results are briefly summarized below.

We have discovered a new phase of ZrO_2 while investigating changes in the degree of transformation toughening in magnesia-partially stabilized zirconia at low temperatures (Section 2). A single cooling cycle to temperatures below ~ -100°C was found to cause severe degradation of room-temperature mechanical properties. The fracture toughness was reduced from ~ 13 MPa•m$^{1/2}$ to ~ 6 MPa•m$^{1/2}$, tensile stress-strain response became linear up to failure instead of being nonlinear, and the R-curve characteristics and flaw tolerance of the high-toughness Mg-PSZ was lost. However, the original high-toughness properties were restored by heating to 400°C. In situ Raman spectroscopy and optical observations during cooling, as well as room-temperature x-ray diffraction, were used to monitor structural changes and to correlate them with these changes in mechanical properties. The degradation in mechanical properties coincided with the transformation of most of the tetragonal precipitates that are responsible for toughening to a new phase with unit cell volume larger than that of tetragonal phase, but smaller than that of the monoclinic phase. The new phase was stable upon heating to at least 300°C, but it transformed back to the tetragonal structure at 400°C.

Although a general understanding exists of the mechanics of crack tip shielding by a transformation zone, and there is a formulation for calculating the toughening quantitatively once the zone shape and transformation strains are specified, there are large

gaps in our knowledge of the factors that are critical for designing optimum materials. These include the microstructural characteristics that dictate the zone shape and size, the nature of the transformation strain within the zone (i.e., whether both dilation and shear are present), and the role of continuously variable volume fraction of transformation across the zone, rather than a step profile. Progress in these areas is presently hindered by lack of knowledge of the critical stress state needed for triggering the transformation and limitations of methods for experimentally measuring these important characteristics of the zone.

In Section 3, a new approach for obtaining the nature and distribution of transformation strains in a zone surrounding a surface-breaking crack is described. This method involves measuring out-of-plane distortions of the free surface at various locations across the transformation zone adjacent to the crack and comparing the measurements with the distortions calculated by modeling the zone as a set of nested inclusions. A convenient procedure was devised for adjusting the distribution of transformation strains in the inclusions and fitting the calculated profiles to experimentally measured values to allow the strain distribution to be deduced. The Raman microprobe was also used to measure variations of monoclinic and tetragonal phase content within the zone. Good agreement was found between these measurements and the distribution obtained from surface uplift measurements. The degree of transformation was found to be inhomogeneous, being maximum near the crack and decreasing linearly or faster with distance from the crack plane. Over most of the transformation zone, the transformation-strains were dilational (i.e., shear component relieved by twinning), but there was also evidence that a significant shear strain persists near the crack plane.

In Section 4, factors that influence nucleation and stabilization of the transformation in various ZrO_2-containing materials are examined. Direct observations of reversible and permanent transformation in various stress states are presented, and the thermodynamics of the transformation are discussed with special reference to factors that influence the nucleation and stabilization of the monoclinic product phase. The aspect ratio of the transformed particle was identified as a factor that influences the stability of the transformation and the load at which stress-induced transformation product becomes stabilized rather than being thermoelastically reversible. Mechanisms based on this idea were consistent with observations of reversible and irreversible transformation in several ZrO_2-based materials.

In the studies of microstructural development during sintering, the eventual aim is to develop high temperature transformation-toughened systems such as $HfO_2/ZrO_2/TiO_2$ by processing in multiphase regions to control microstructure and control grain growth. Initial experiments, aimed at understanding mechanisms involved, have been done using the system ZrO_2/Y_2O_3 in which we know we can retain the tetragonal phase by processing in a two-phase region (Section 5). Specimens with extremely uniform initial compositional distribution were fabricated from a metastable precursor, obtained by mixing solutions of zirconium acetate and yttrium nitrate and drying to form a glass which was then heat-treated to decompose the organic constituents and to allow densification of the oxide. Compositions in the range 1 to 5 mole%, Y_2O_3 (where grain growth is known to be inhibited) were heat-treated for various periods in the temperature range 1400-1600°C, for which these compositions should lie in a two-phase tetragonal (low Y_2O_3) cubic (high Y_2O_3) region. X-ray, TEM and SEM studies were done to quantify grain growth rates and relate these to microstructural evolution (Section 5). It has become clear that the partitioning phenomenon in the two-phase region is more complex than previously thought. Measurements of compositional variations (using analytical transmission electron microscopy) within and between grains after various heat-treatment periods indicate that the partitioning begins with small composition fluctuations between grains rather than by nucleation of grains with the two equilibrium compositions. Phase partitioning was observed to be extremely sluggish, requiring many weeks at normal sintering temperatures to establish equilibrium phases. Moreover, grain growth was observed to be extremely slow during the very early stages of partitioning. Therefore, it appears that a small difference in Y_2O_3 content in adjacent grains serves to inhibit grain boundary movement and hence grain growth. It is known that the lattice parameters of the tetragonal structure vary with Y_2O_3 content. On the basis of these observations we have postulated that movement of a grain boundary separating grains of slightly different composition would generate strain energy because of the lattice parameter mismatch. An analytical model has been developed to account for the inhibiting effect of the strain energy on grain growth. The model predicts rapid growth of the grains to a stable size, consistent with experimental observations, and suggests that the key to similar grain growth control in other two-phase systems lies in selecting alloy systems in which there is a similar variation of lattice parameter with alloying species.

2. STRUCTURAL AND MECHANICAL PROPERTY CHANGES IN TOUGHENED ZIRCONIA CERAMICS AT LOW TEMPERATURES

To be submitted to J. Am. Ceram. Soc.

Rockwell International
Science Center

STRUCTURAL AND MECHANICAL PROPERTY CHANGES IN TOUGHENED
ZIRCONIA CERAMICS AT LOW TEMPERATURES

D.B. Marshall

Rockwell International Science Center
Thousand Oaks, CA 91360

ABSTRACT

The mechanical properties of high-toughness magnesia-partially stabilized zirconia were found to be dramatically altered by a single cooling cycle between room temperature and $-196°C$. Raman spectroscopy and x-ray diffraction were used to correlate the changes in mechanical properties with structural changes at temperatures below $\sim -100°C$. Most of the tetragonal precipitates that are responsible for toughening transformed to a new phase with unit cell volume intermediate between those of the tetragonal and monoclinic phases. The new phase was stable with heating to $300°C$, but it transformed back to the tetragonal structure when heated to $400°C$.

J8865D/sn

1. INTRODUCTION

Zirconia-containing ceramics can be toughened dramatically by the martensitic tetragonal-to-monoclinic transformation in localized zones around cracks.[1-13] However, high toughening requires a very narrow range of microstructures in which ZrO_2 grains or precipitates are on the verge of spontaneous transformation. Since the transformability of constrained ZrO_2 particles is sensitive to the degree of undercooling from the unconstrained M_s (martensitic start) temperature, both the degree of toughening and the stability of the microstructure are expected to be very sensitive to temperature changes.

The highest toughness ZrO_2 ceramics are from the magnesia-partially stabilized zirconia system (Mg-PSZ). In optimally aged materials, with toughness up to 18 MPa·m$^{1/2}$, the tetragonal precipitates are so close to spontaneous transformation at room temperature that a fraction do transform during cooling, and others begin to transform under applied tensile stresses as low as 300 MPa. The purpose of this paper is to examine whether cooling below room temperature causes further transformation of these precipitates, and thereby a loss of toughening at cryogenic temperatures, or even more importantly, degradation of room-temperature mechanical properties after a single cooling cycle. Swain[14,15] has shown previously that the fracture toughness of such materials is reduced at liquid N_2 temperature, and that thermal expansion measurements indicate a volume increase in the temperature range -80 to -100°C. We will show that cooling does indeed cause a transformation, but that the transformation product is not the normal monoclinic structure. Instead, it appears to be a new phase of ZrO_2 that has not been observed previously.

2. EXPERIMENTAL

The material of primary interest in this study is the high-toughness, 9 mole% MgO-partially stabilized zirconia (Mg-PSZ), which was fabricated by sintering at 1700°C, with controlled cooling to room temperature, followed by subeutectoid heat treatment at 1100°C (Table 1) This optimally aged material contained lens-shaped, MgO-depleted precipitates, ~ 200 nm in diameter, in a fully stabilized (MgO-rich) cubic matrix. Most of the precipitates were of the tetragonal structure, but some (~ 13 vol%) transformed to the monoclinic phase during cooling. Some of this material was overaged by heating to 1400°C for two days, resulting in transformation of all precipitates to monoclinic structure upon cooling.

Several other related materials, with different compositions and heat treatments, were also tested for comparison (Table 1). One series was 9 mole% MgO-PSZ that had been heat treated at 1100°C for 0, 7 or 24 h to give materials with a range of transformation toughening. The room-temperature mechanical properties of these materials were reported in detail elsewhere.[16] The material with 24 h heat treatment was indistinguishable from the high toughness material mentioned above. In tensile loading of specimens with polished surfaces, the stress-strain response was nonlinear because of stress-induced transformation and microcracking at stresses above ~ 300 MPa. The sequence of damage development is shown in Fig. 1. Stresses below 300 MPa caused reversible surface roughening, which was correlated with tetragonal-to-monoclinic transformation, whereas higher stresses resulted in permanent transformation and the formation and stable growth of microcracks to lengths up to 1 mm. The stable crack growth was attributed to an increasing crack resistance curve (R curve) with increasing crack extension. The steady-state fracture toughness was ~ 13 MPa·m$^{1/2}$, and transformation zones ~ 100 μm in width around cracks were readily observed because of surface uplift

due to transformation strains (Fig. 1). The material with 9 h heat treatment had a steady-state fracture toughness of ~ 9 MPa·m$^{1/2}$ and also exhibited nonlinear stress-strain response, R-curve behavior and transformation zones around cracks, but all less extensive than in the 24 h heat-treated material (Fig. 1d) The material that was not heat treated at 1100°C did not show nonlinear load-deflection response or stable microcrack growth during failure testing, but a transformation zone around the crack that caused failure was observed (Fig. 1e). Other materials tested were a 14 mole% MgO ZrO$_2$ which was all stabilized cubic phase, and a 3 mole% MgO-PSZ which contained tetragonal precipitates that cannot be transformed to monoclinic phase by applied stress (transformation zones were not seen around cracks in this material).

Structural changes occurring during cooling to -196°C were monitored in situ for some materials by optical microscopy and Raman spectroscopy, using a small cooling stage with a quartz window. Optical microscopy was done with Nomarski interference to allow detection of surface distortion produced by transformation strains. Raman spectroscopy was done using a microprobe with spot size of ~ 20 µm when the specimen was in the cooling stage and ~ 1 to 2 µm otherwise.

Changes in room-temperature mechanical properties after cooling to -196°C were evaluated by loading beams (approximately 3 x 3 x 40 mm) in flexure using a fixture on the stage of an optical microscope. The polished tensile surface was observed during loading and strains were measured using strain gauges attached to the specimens.

3. RESULTS

3.1   Optical Observations

The polished surface of a peak toughness Mg-PSZ before and after cooling to liquid N_2 is shown in Fig. 2. Surface distortions similar to those produced by stress-induced tetragonal-to-monolinic transformation (Fig. 1) are evident in the Nomarski interference micrographs. Quantitative measurements using conventional interference microscopy indicated that the amplitude of the distortion (~ 50 nm) was larger than that due to the reversible transformation at low applied stresses (~ 20 nm) (Fig. 1(A)), but smaller than that due to permanent transformation (~ 100 to 200 nm) (Fig. 1(B)).

The stress-induced transformation causes relatively uniform uplift of areas that span several grains (presumably, those grains most favorably oriented relative to the applied stress), whereas cooling to liquid N_2 caused general uplift of most of the surface except for isolated areas ~ 20 μm diameter. These areas of surface depression were found to correspond with regions, usually near the centers of grains, that contained comparatively large precipitates which would have transformed to monoclinic structure during cooling (Fig. 2). Formation of these large precipitate regions has been discussed elsewhere.[17]

During in-situ experiments using the cooling stage, the distortions in Fig. 2 were observed to develop over the temperature range -80°C to -120°C and then remain unchanged as the temperature was lowered to -196°C and increased to +96°C. Subsequent heating for 10 min at 300°C also left the surface distortion unaltered. However, after 3 min at 400°C, most of the distortions disappeared. The temperature range over which surface uplift developed coincides with the temperature range over which Swain[15]

previously observed a volume increase from thermal expansion measurements. The persistence of the volume expansion upon heating to room temperature is also consistent with Swain's results.

Similar response was observed in the intermediate toughness Mg-PSZ, but the surface distortions appeared at lower temperatures (-120°C to -160°C), again consistent with Swain's thermal expansion measurements. Comparison of polished surfaces of the other materials in Table I did not reveal any surface distortions.

3.2   Raman Spectroscopy

Raman spectra from the high-toughness Mg-PSZ before and after immersion in liquid N_2 are shown in Fig. 3. Also shown for comparison are spectra from 14% Mg-ZrO_2 (cubic structure) and the overaged PSZ (cubic matrix with monoclinic precipitates). The spectrum obtained after cooling to -196°C contains at least eleven peaks in the range 100-700 cm^{-1} that were not present before cooling, and the original tetragonal peaks are all present, but greatly reduced in intensity. Two of the new peaks (338 and 480 cm^{-1}) coincide with peaks of the monoclinic phase (Fig. 3d), but the remaining nine do not belong to any of the tetragonal, monoclinic or cubic phases. Moreover, there are several strong peaks in the monoclinic spectrum of Fig. 3c that do not appear in Fig. 3b (e.g., 177, 384, 624 cm^{-1}). Therefore, cooling to -190°C caused transformation of most of the tetragonal precipitates to a new phase that is not the monoclinic structure.

Results from in-situ Raman measurements during cooling of the high-toughness Mg-PSZ are shown in Fig. 4. The new phase forms over the temperature range -80 to -120°C, corresponding to the temperature range over which volume expansions and surface roughening were observed. Moreover, after the heat treatment at 400°C, when the

surface distortions disappeared, the Raman spectrum returned to the same as before cooling (Fig. 5). In-situ measurements from the intermediate toughness Mg-PSZ yielded similar results, with the transformation occurring over the range -120°C to -160°C, again consistent with the surface roughening and thermal expansion results. Raman measurements from the other materials in Table 1 did not reveal any changes in the spectra before and after immersion in liquid N_2.

3.3 X-Ray Measurements

Changes were observed in the x-ray diffraction patterns from the high-toughness Mg-PSZ after cooling to liquid N_2. Diffraction patterns obtained at room temperature before and after cooling are compared in Fig. 6. Before cooling, this material contained ~ 13% monoclinic precipitates, ~ 30% tetragonal precipitates, and the remainder cubic matrix. After cooling in liquid N_2, there was no change in the intensities of the monoclinic pea. .s (e.g., (111) and (11$\bar{1}$)), but the tetragonal peaks nearly disappeared (e.g., (002), (022) and (113)) and some new peaks appeared, as indicated by shading in Fig. 6 and listed in Table 2. A diffraction pattern from the overaged Mg-PSZ (i.e., monoclinic precipitates, cubic matrix) is also shown in Fig. 6a for comparison. It is clear that the new peaks that occur after cooling do not belong to the monoclinic phase. Moreover, the new peaks cannot be accounted for by any of the other reported phases of ZrO_2 (orthorhombic[18,19] and rhombohedral[20]) or by the Mg-rich δ-phase[21] that exists in the high-toughness material.

Preliminary attempts were made to use cell-fitting routines with the data of Table 2 to determine the cell dimensions. However, these were not successful, most likely because of overlap of many low-order peaks with the cubic, tetragonal and monoclinic peaks.

3.4   Mechanical Properties

The steady-state fracture toughness of the high-toughness Mg-PSZ was recently measured at -196°C and found to be reduced from ~ 13 MPa·m$^{1/2}$ at room temperature to ≈ 7 MPa·m$^{1/2}$. This toughness is higher than that of the overaged material (3 MPa·m$^{1/2}$, Table 1), indicating that, although the degree of transformation toughening was reduced at -196°C, it was not completely eliminated. The steady-state toughness is similar to that of the low toughness Mg-PSZ (Table 1) that was not given the subeutectoid heat treatment.

3.4.1   Flexural Loading

Flexural loading of the high-toughness Mg-PSZ after cooling to -196°C and warming to room temperature resulted in linear stress-strain curve to failure and strength of 520 MPa. There was no permanent transformation or stable microcrack growth during loading, although in one experiment a microcrack ~ 50 μm in length initiated and was stable for ~ 2 seconds at constant load before extending unstably. Post-failure examination of the surface that was stressed in tension revealed the presence of a transformation zone around the crack that caused failure, and around several cracks that branched from the main one (Fig. 7). The width of the transformation zone was substantially smaller (~ 10 μm) than in the specimen which had not been cooled to -196°C. The transformation zone width was about the same as in the low toughness Mg-PSZ that was not heat treated at 1100°C (Fig. 1e and Table 1), implying that the steady-state toughness is ≈ 6 MPa·m$^{1/2}$ and therefore similar to the toughness measured at -196°C.

After heating to 600°C for 3 min, the mechanical behavior characteristic of the high-toughness Mg-PSZ was restored. During loading, permanent transformation

developed and stable microcracks grew to ~ 1 mm before failure. The stress-strain curve was nonlinear, with the apparent flexural strength of 600 MPa and a true failure stress of 400 MPa. Stable microcracks and permanent transformation, as well as a larger transformation zone around the main crack, are evident in the post-failure micrograph of Fig. 8 (cf. Fig. 1 for specimen not subject to cooling-heating cycle).

3.4.2   Indentation Experiments

Indentations (300 N Vickers) made in the high-toughness Mg-PSZ before and after cooling to -196°C and after heating to 600°C are compared in Fig. 9(a-f). Also included for comparison in Fig. 9(g) and (h) are indentations in the series of subeutectoid heat-treated Mg-PSZ. After a cooling cycle to -196°C and back to room temperature the area of transformation induced by indentation (Fig. 9e) was reduced to a size similar to that in the low toughness Mg-PSZ (Fig. 9h). After subsequent heating to 600°C and cooling to room temperature, the transformation zone size was similar to that in the original material (Fig. 9f). These results indicate that the propensity for stress-induced transformation decreases upon cooling to -196°C and is restored by heating to 600°C, consistent with the results obtained in flexural loading.

The micrographs in Figs. 9a and b also afford a convenient comparison of the relative volume changes associated with the stress-induced tetragonal-to-monoclinic transformation and the low temperature transformation from tetragonal structure to the new phase. From the micrographs corresponding both to cooling to -196°C after indentation (Fig. 9b and d) and indentation after cooling to -196°C (Fig. 9e), it is clear that the total volume change during cooling is smaller than from complete tetragonal-to-monoclinic transformation. These results are consistent with the measurements of Section 3.1.

4. DISCUSSION

The results of the previous section have directly linked the formation of a new phase of ZrO_2 to dramatic changes in mechanical properties of high-toughness Mg-PSZ. A single cooling cycle from room temperature to -100°C results in transformation of tetragonal precipitates to the new phase, with an accompanying reduction in fracture toughness and elimination of both nonlinear stress-strain response and R-curve behavior. However, the original high-toughness properties can be restored by a subsequent heating cycle to 400°C, which causes transformation of the new phase back to the tetragonal structure.

The detailed structure of the new phase has not been determined. The Raman results rule out the monoclinic, tetragonal and cubic structures of ZrO_2, as well as the high-pressure orthorhombic phase.[22] The x-ray results also rule out these phases, as well as the rhombohedral phase. However, we can deduce from the observations of surface distortions caused by cooling, indentation, and crack tip transformation zones, that the unit cell volume of the new phase is larger than that of the tetragonal structure, but smaller than the monoclinic cell volume. These qualitative results are consistent with the thermal expansion data of Swain,[15] who measured a linear strain increase of ~ 0.15% over the temperature range in which we observe transformation to the new phase. If this strain resulted from all of the tetragonal precipitates transforming to the new phase (volume fraction of tetragonal phase ≈ 0.3), the dilation strain associated with the transformation would be 1.5%, i.e., approximately one-third of the tetragonal-to-monoclinic transformation strain (~ 4.5%). Both the Raman spectroscopy and the x-ray diffraction suggest, at least qualitatively, that most of the tetragonal precipitates did transform to the new phase during cooling to -196°C and remained transformed upon warming to room temperature. However, these results are qualitative and a smaller fraction of transforming precipitates would correspond to a larger transformation strain.

14
J8865D/sn

Although the degree of transformation toughening is reduced by the cooling cycle, toughening is not eliminated altogether. A question of central importance to understanding the relation of the new phase to mechanical properties is whether the residual transformation toughening arises from the surviving fraction of tetragonal precipitates, with the new phase not being at all transformable to monoclinic in the stress field near the crack tip, or alternatively, whether the new phase undergoes stress-induced transformation to the monoclinic structure and provides transformation toughening. Circumstantial evidence can be found in our results to support either of these alternatives. The absence of transformation during cooling in the low toughness Mg-PSZ and in the 3% Mg-PSZ implies that, in the high-toughness Mg-PSZ, the precipitates that transform to the new phase during cooling that are the same ones that are most easily transformed by stress (and which give rise to the large toughening). Raman measurements from regions adjacent to cracks in the high-toughness Mg-PSZ indicate that only some of the tetragonal precipitates (approximately half) transform to monoclinic and that the fraction of tetragonal phase remaining in the crack tip zone is larger than the fraction remaining after cooling to -196°C (compare Figs. 3b and 10). These results imply that all of the tetragonal precipitates remaining after cooling should also remain untransformed in the crack tip zone. In this case, the crack tip transformation zone would arise from stress-induced transformation from the new phase to monoclinic. However, the observations that a crack tip transformation zone is formed in the low toughness Mg-PSZ but no transformation occurs during cooling would lead to the opposite conclusion.

An attempt was made to identify the source of residual toughening after cooling to -196°C by comparing Raman spectra from areas adjacent to, and remote from, the crack that caused failure in flexural loading (Fig. 11). An increase in monoclinic phase is

evident (shaded peaks) confirming that it is indeed transformation to the monoclinic phase that gives rise to the transformation zone. However, the sensitivity is not sufficiently high to determine whether this transformation corresponded to a decrease in tetragonal phase or a decrease of the new phase.

5. CONCLUSIONS

A single cooling cycle for high-toughness Mg-PSZ to temperatures below ~ -100°C causes severe degradation of room-temperature mechanical properties. The fracture toughness is reduced from ~ 13 MPa•m$^{1/2}$ to ~ 6 MPa•m$^{1/2}$, tensile stress-strain response becomes linear up to failure instead of being nonlinear, and the R-curve characteristic of the high-toughness Mg-PSZ is lost. However, the original high-toughness properties are restored by heating to 400°C.

The degradation in mechanical properties coincides with the transformation of most of the tetragonal precipitates to a new phase with unit cell volume larger than that of the tetragonal phase, but smaller than that of the monoclinic phase. The new phase is stable upon heating to at least 300°C, but at 400°C (for 3 min), it transforms back to the tetragonal structure.

ACKNOWLEDGEMENTS

REFERENCES

1. R.S. Garvie, R.H.J. Hannink and R.T. Pascoe, "Ceramic Steel?," Nature 258 (5537) 703-704 (1975).

2. D.L. Porter and A.H. Heuer, "Mechanisms of Toughening Partially Stabilized Zirconia," J. Am. Ceram. Soc. 60 (3-4), 183-84 (1977).

3. F.F. Lange, "Transformation Toughening: Part 5. Effect of Temperature and Alloy on Fracture Toughness," J. Mat. Sci. 17, 255-263 (1982).

4. F.F. Lange, "Transformation Toughening: Part 4. Fabrication, Fracture Toughness and Strength of Al_2O_3-ZrO_2 Composites," J. Mat. Sci. 17, 247-54 (1982).

5. N. Claussen and M. Ruhle, "Design of Transformation Toughened Ceramics," pp. 137-63 in Advances in Ceramics, Vol. 3, Ed., A.H. Heuer and L.W. Hobbs, Am. Ceram. Soc. (1981).

6. M.V. Swain, R.H.J. Hannink and R.C. Garvie, pp. 339-54 in Fracture Mechanics of Ceramics, Vol. 6, edited by R.C. Bradt, A.G. Evans, D.P.H. Hasselman and F.F. Lange, Plenum, NY (1983).

7. R.H.J. Hannink, "Growth Morphology of the Tetragonal Phase in Partially Stabilized Zirconia, "J. Mat. Sci. 13, 2487-96 (1978).

8. R.H.J. Hannink, K.A. Johnston, R.T. Pascoe and R.C. Garvie, pp. 116-136 in Advances in Ceramics, Vol. 3, edited by A.H. Heuer and L.W. Hobbs, Am. Ceram. Soc. (1981).

9. M.V. Swain and R.H.J. Hannink, "R-Curve Behavior in Zirconia Ceramics," in Science and Technology of Zirconia II, Advances in Ceramics, Vol. 12, eds., N. Claussen, M. Ruhle and A.H. Heuer, Am. Ceram. Soc., Columbus (1984), pp. 225-239.

10. M.V. Swain, "Inelastic Deformation of Mg-PSZ and Its Significance for Strength-Toughness Relationships of Zirconia Toughened Ceramics," Acta. Met. 33 (11), 2083-91 (1985).

11. D.B. Marshall, "Strength Characteristics of Transformation-Toughened Zirconia," J. Am. Ceram. Soc. 69 (3), 173-180 (1986).

13. M.J. Ready and A.H. Heuer, "Crack Development in Transformation-Toughened Mg-PSZ," in Advanced Structural Ceramics, Proc. MRS Fall Meeting, Boston (1986).

13. M.J. Ready and A.H. Heuer, "On the Annealing of Test Specimens of High Toughness Mg-PSZ," J. Am. Ceram. Soc., in press.

14. S. Veitch, M. Marmach and M.V. Swain, "Strength and Toughness of Mg-PSZ and Y-TZP Materials at Cryogenic Temperatures," in Advanced Structural Ceramics, Proc. MRS Fall Meeting, Boston (1986).

15. M.V. Swain, private communication.

16. D.B. Marshall and M.V. Swain, "Crack Resistance Curves in Magnesia-Partially-Stabilized Zirconia," J. Am. Ceram. Soc., in press.

17. R.R. Hughan and R.H.J. Hannink, "Precipitation During Controlled Cooling of Magnesia-Partially-Stabilized Zirconia," J. Am. Ceram. Soc. 69 (7), 556-63 (1986).

18. A.H. Heuer, L.H. Schoenlein and S. Farmer, "New Microstructural Features in Magnesia-Partially-Stabilized Zirconia (Mg-PSZ), in Science of Ceramics 12, Cermurgica, Italy, pp. 257-267.

19. B.C. Muddle and R.H.J. Hannink, "Phase Transformation Involving an Orthorhombic Phase in MgO-PSZ,"

20. H. Hasegawa, T. Hioki and O. Kamigaito, "Cubic to Rhombohedral Phase Transformation in Zirconia by Ion Implantation," J. Mat. Sci. Lett. 4, 1092-94 (1985).

21. R.H.J. Hannink and M.V. Swain, "Magnesia-Partially-Stabilized Zirconia: the Influence of Heat Treatment on Thermomechanical Properties," J. Aust. Ceram. Soc. 18 (2), 53-62 (1982).

22. A. Arashi and M. Ishigame, "Raman Spectroscopic Studies of the Polymorphism in ZrO_2 at High Pressures," Phys. Stat. Sol. (a) 71, 313-321 (1982).

Table 1

Materials Tested

Material	Mole% MgO	1100°C	1400°C	Steady State Toughness (MPa·m$^{1/2}$)	Apparent Flexural Strength (MPa)	True Strength (MPa)
High Toughness[a]	9	By manufacturer[a]		13	620	400
Overaged[a]			48	3		
High Toughness[b]	9	24		13	620	400
Intermediate[b] Toughness	9	7		10	700	600
Low Toughness[b]	9	0		6	540	540
14% MgO-ZrO$_2$[b]	14					
3% Mg-PSZ[b]	3					

a. Nilcra
b. Specimens kindly supplied by M.V. Swain

Table 2

X-Ray Diffraction Peaks that Appeared in High-Toughness Mg-PSZ After
Cooling in Liquid N_2 (Cu-Kα Radiation)

2θ (deg)	Relative Intensity	2θ (deg)	Relative Intensity
23.0	Weak	53.3	Weak
24.5	Strong	55.4	Weak
34.15	Strong	58.6	Strong
38.5	Weak	62.7	Strong
39.4	Weak	65.8	Weak
39.8	Weak	67.6	Weak
42.7	Weak	74.7	Weak
43.5	Strong	81.3	Weak
50.0	Strong	89.4	Weak
52.4	Weak		

FIGURE CAPTIONS

Fig. 1   (a)-(c) Nomarski interference micrographs of polished surface of high-tough-
ness Mg-PSZ: (a) during loading with tensile stress 300 MPa; (b) stress
increased to 380 MPa; (c) after failure; (d) intermediate toughness Mg-PSZ
after failure; (e) low-toughness Mg-PSZ after failure.

Fig. 2   Polished surface of high-toughness Mg-PSZ: before (a) and after (b) cooling to
-196°C. Nomarski interference micrographs.

Fig. 3   Raman spectra (room temperature) from high-toughness Mg-PSZ (polished sur-
face) before and after cooling to -196°C, overaged Mg-PSZ (monoclinic and
cubic phases), and 14% Mg-PSZ (fully stabilized cubic phase).

Fig. 4   In situ Raman spectra from high-toughness Mg-PSZ during cooling.

Fig. 5   Raman spectra from high-toughness Mg-PSZ after cooling to -196°C, then
heating to 600°C and cooling to room temperature.

Fig. 6   X-ray diffraction patterns (Cu K-α) from high-toughness Mg-PSZ before and
after cooling to -196°C and from overaged Mg-PSZ.

Fig. 7   Nomarski interference micrograph from tensile surface of a bar of high-tough-
ness Mg-PSZ that was broken in flexure after being cooled to -196°C, warmed
to room temperature and then polished.

Fig. 8   Nomarski interference micrograph from tensile surface of a bar of high-tough-
ness Mg-PSZ that was broken in flexure after being cooled to -196°C, heated
to 400°C for 3 min, cooled to room temperature and then polished.

Fig. 9   (a-f) Vickers indentations (300 N load) in high toughness Mg-PSZ (Nomarski
         interference micrographs)

         (a) As-received, surface polished before indentations width of field 1.65 mm.

         (b) Same indentation as (a) after cooling to -196°C.

         (c) Higher magnification of (a) (note that contrast due to Nomarski interfer-
         ence is lower with this higher power objective lens). Width of field in (c)-(h);
         825 μm.

         (d) Higher magnification of (b).

         (e) Indentation made in another area of the specimen used for (a)-(d), but after
         cooling to -196°C and warming to room temperature.

         (f) Indentation made after cooling to -196°C, heating to 600°C, and cooling to
         room temperature.

         (g) and (h) Vickers indentations (300 N load) in polished surfaces of: (g) high
         toughness Mg-PSZ (24 h at 1100°C) and (h) low toughness Mg-PSZ.

Fig. 10   Raman spectrum from region adjacent to crack in high-toughness Mg-PSZ.

Fig. 11   Raman spectra from regions adjacent to and remote from the crack in Fig. 7
         (high-toughness Mg-PSZ cooled to -196°C, then broken in flexure).

(A)

(B)

Figure 1A,B

24

(C)

(D)

(E)

25 Figure 1C,D,E

(A)

(B)

Figure 2

26
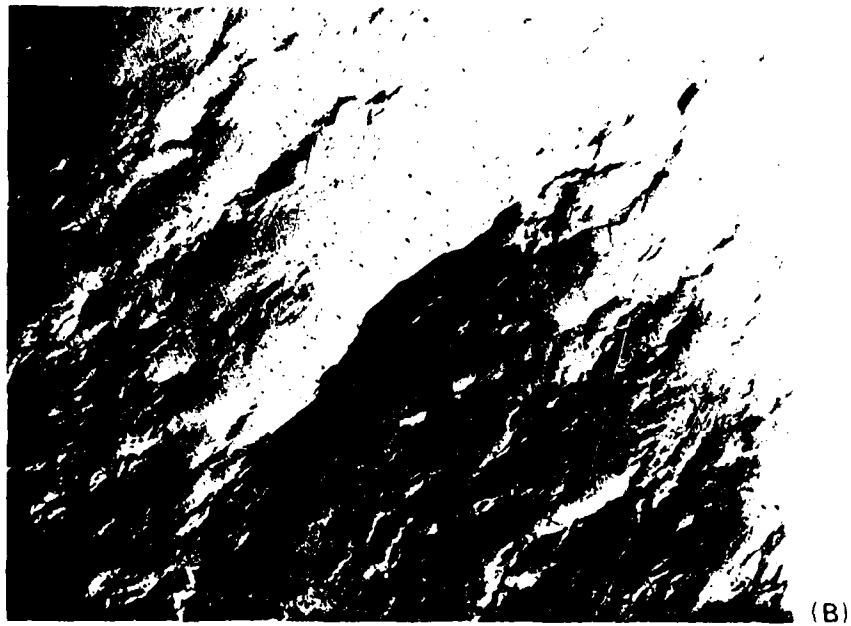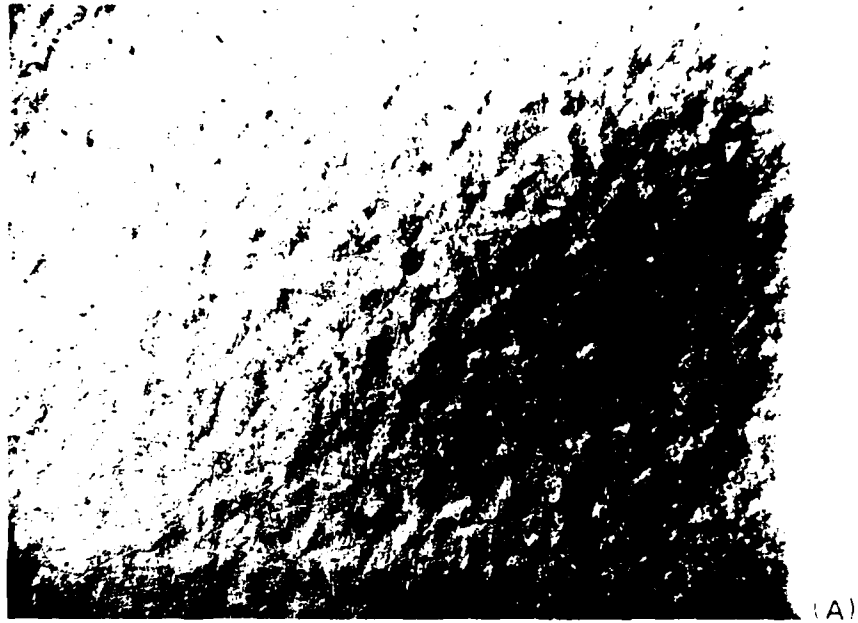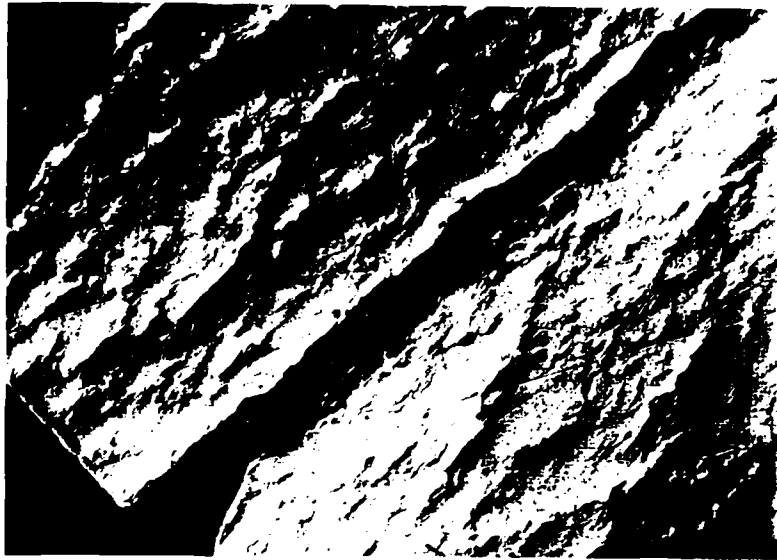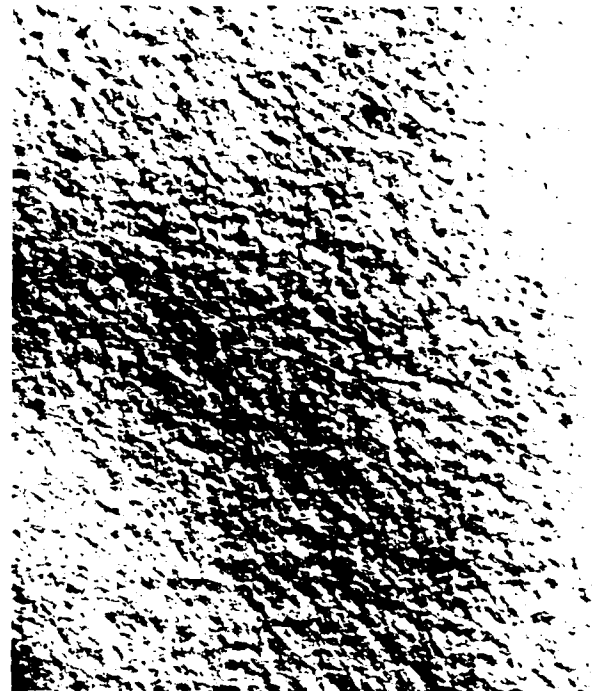
SC42500
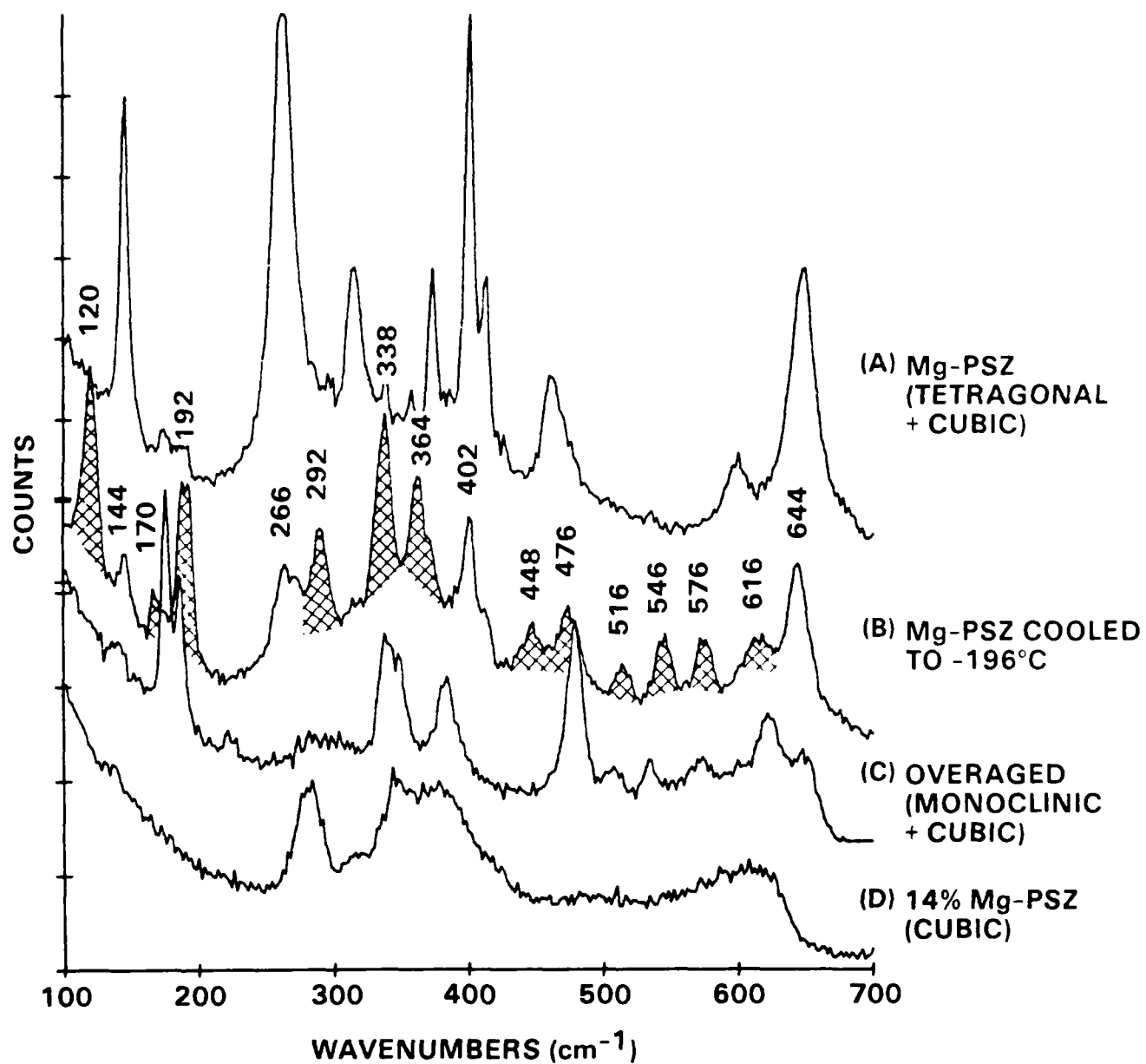
Figure 3
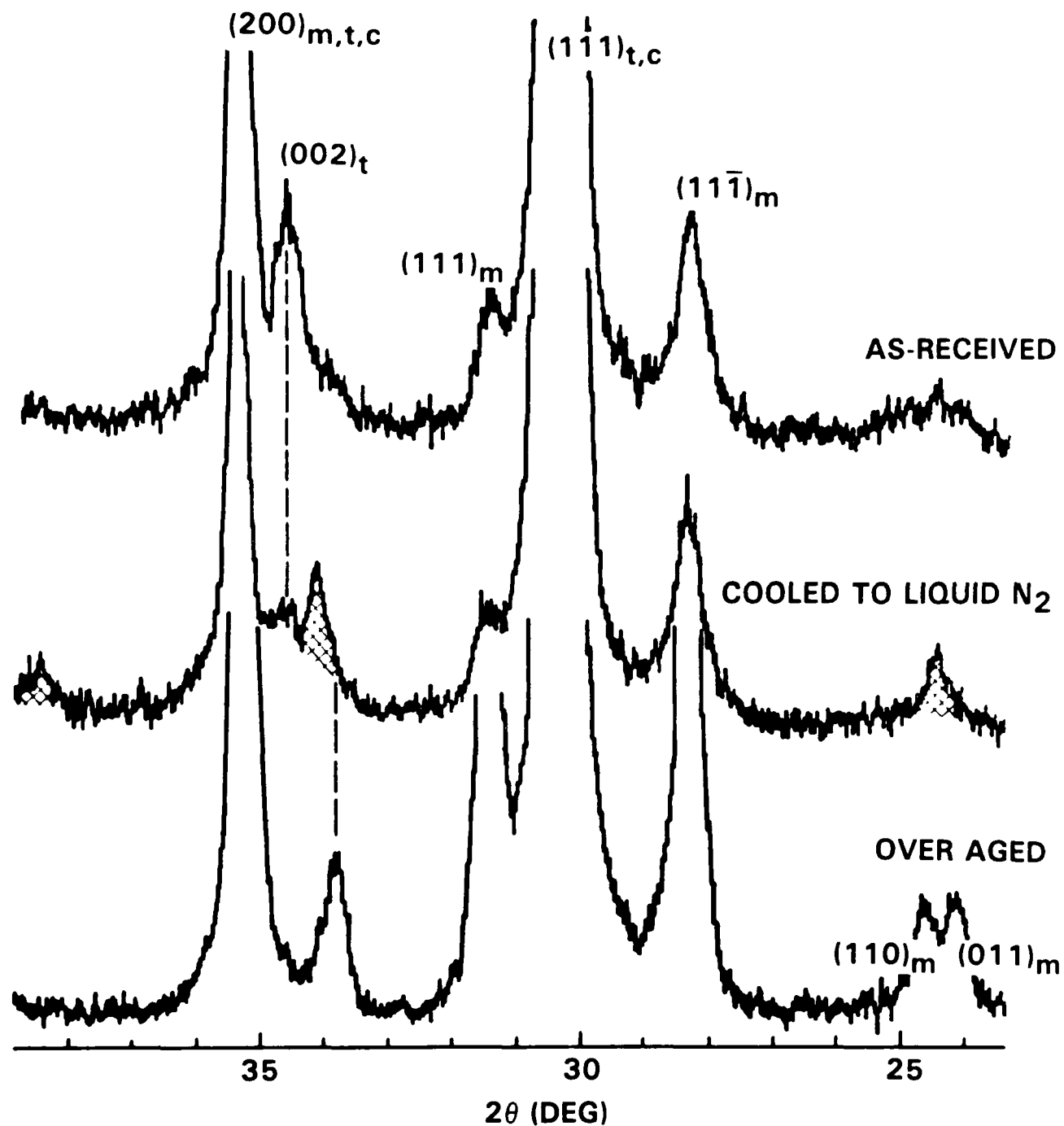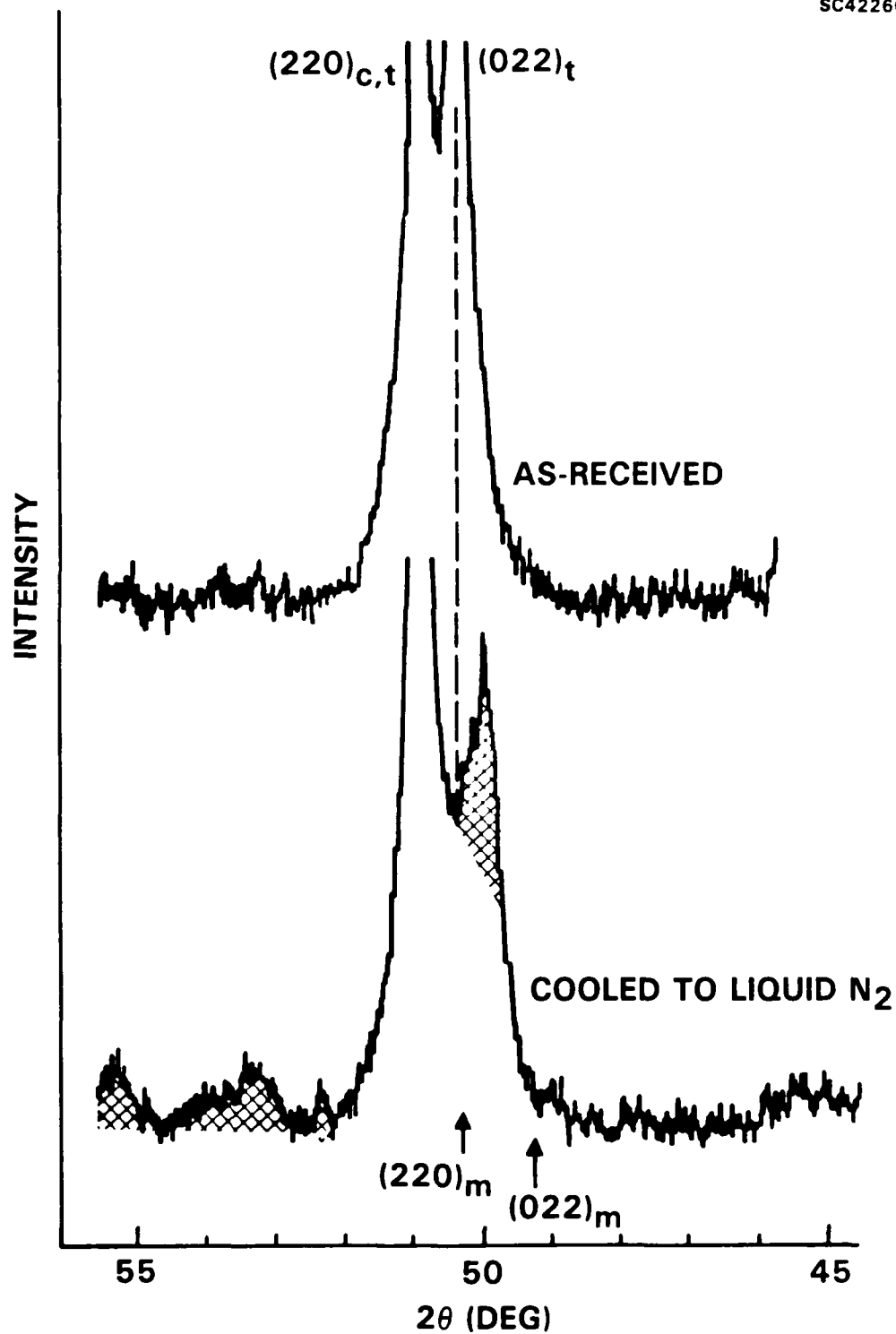
Rockwell International
Science Center
SC42498
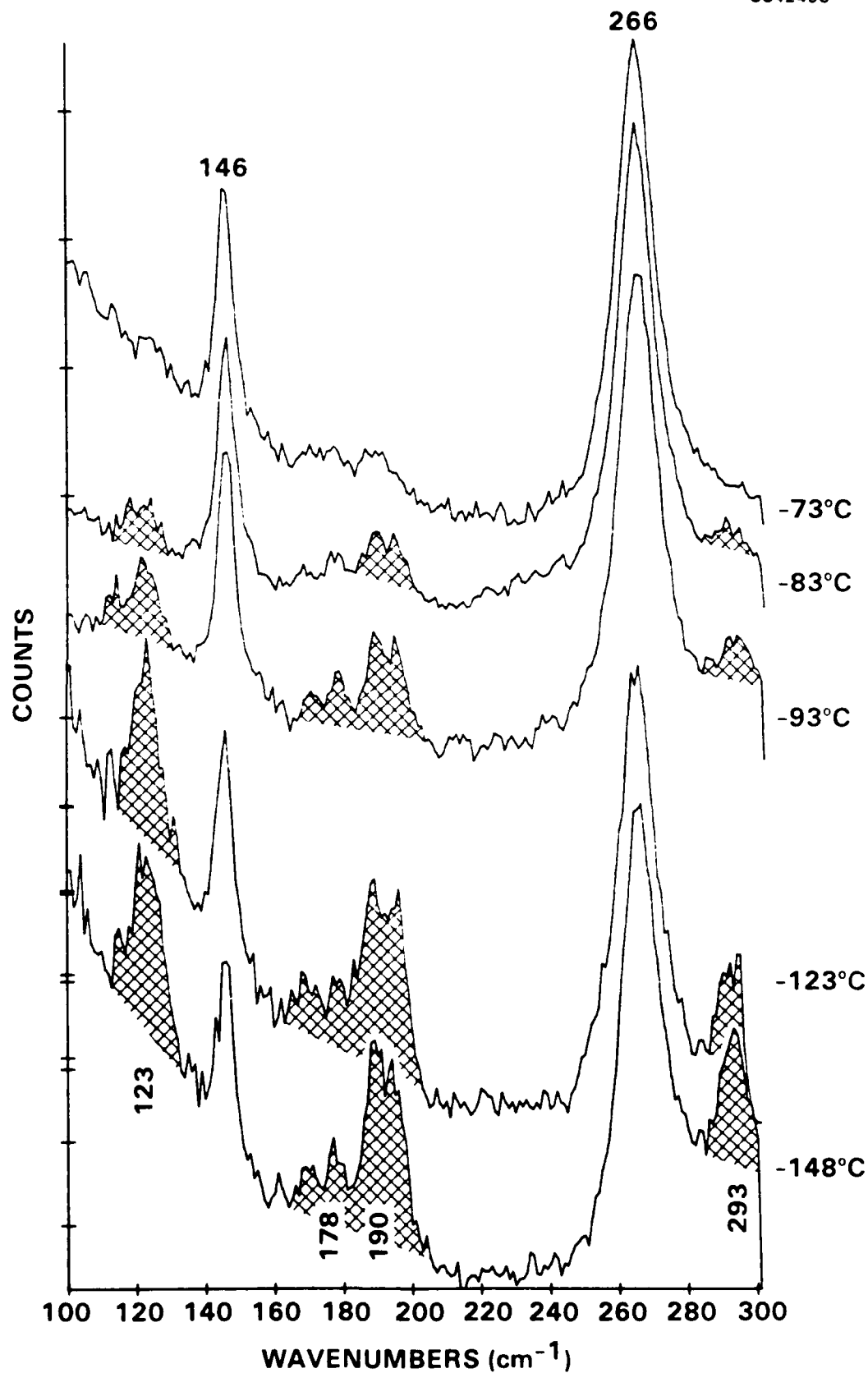
Figure 4

28

Figure 5

29

Figure 6A

30
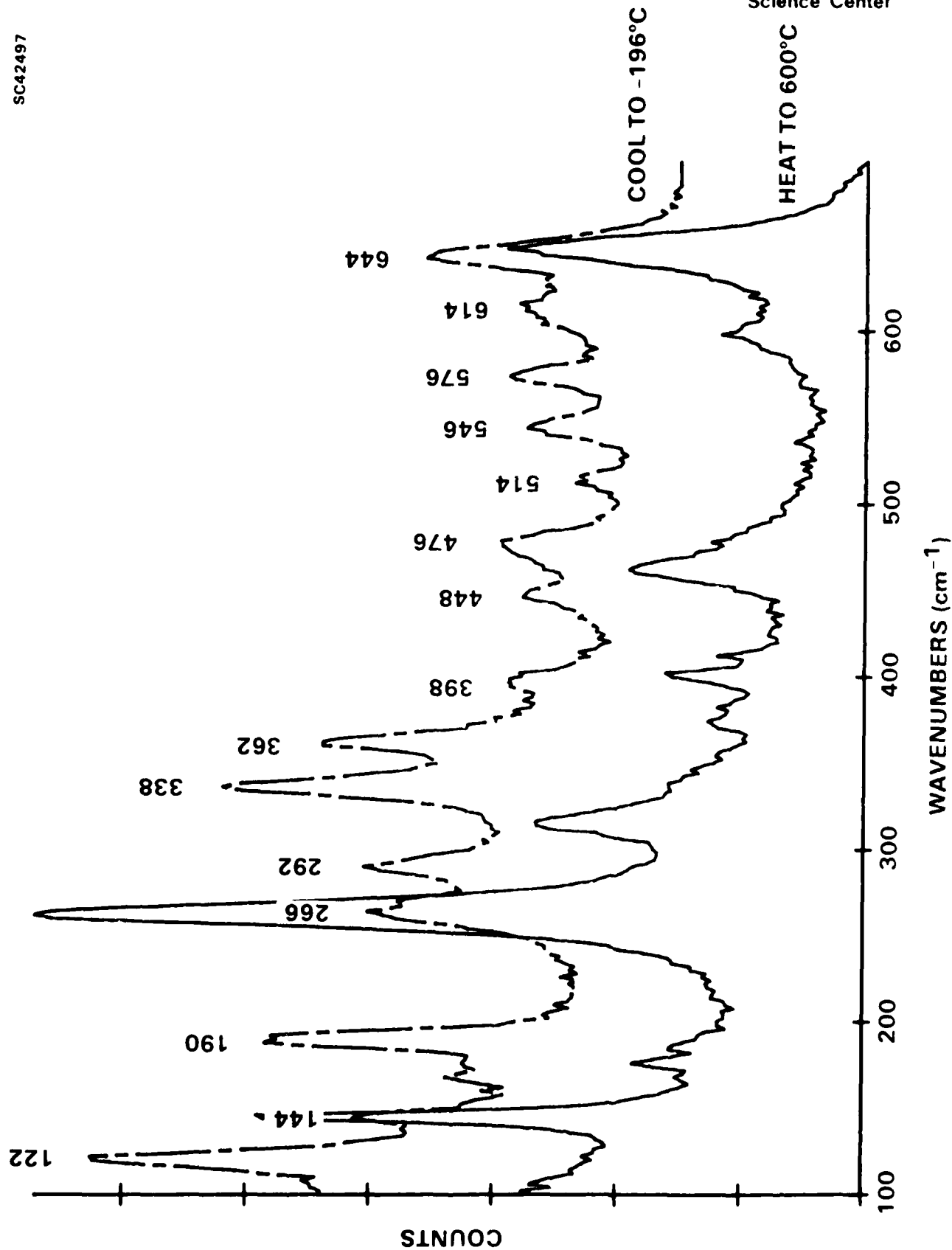
SC42260
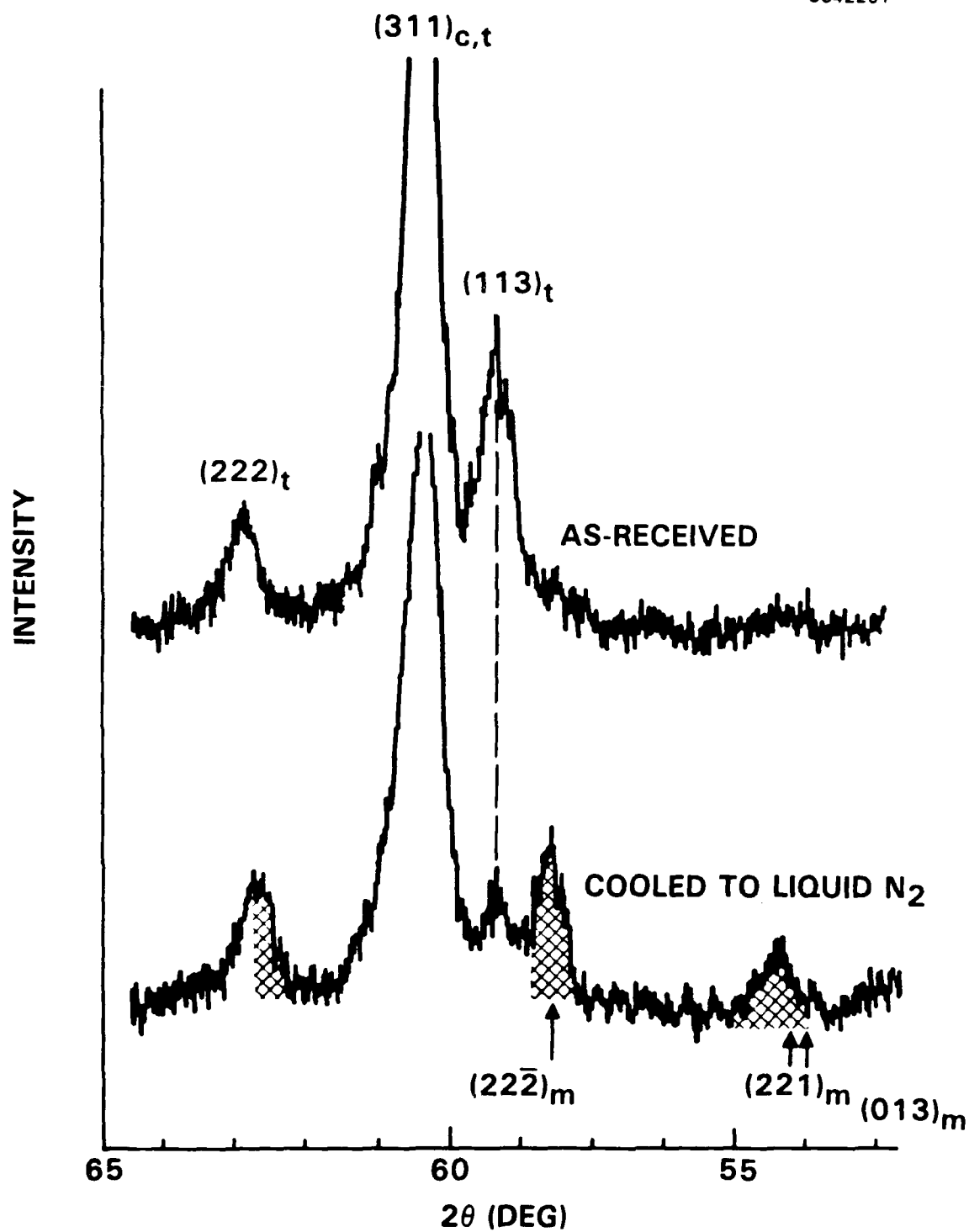
Figure 6B

Figure 6C

Figure 7

Figure 8
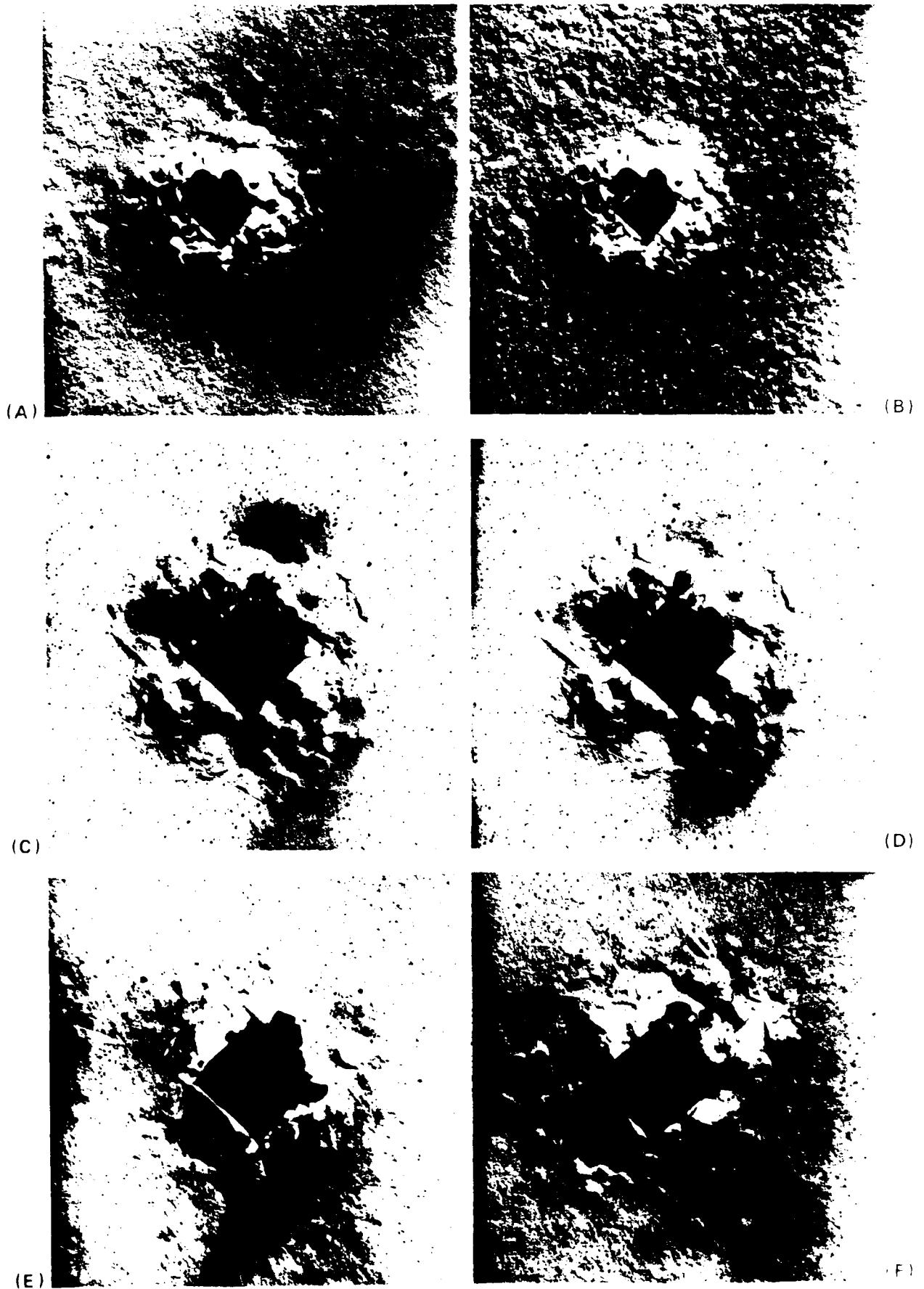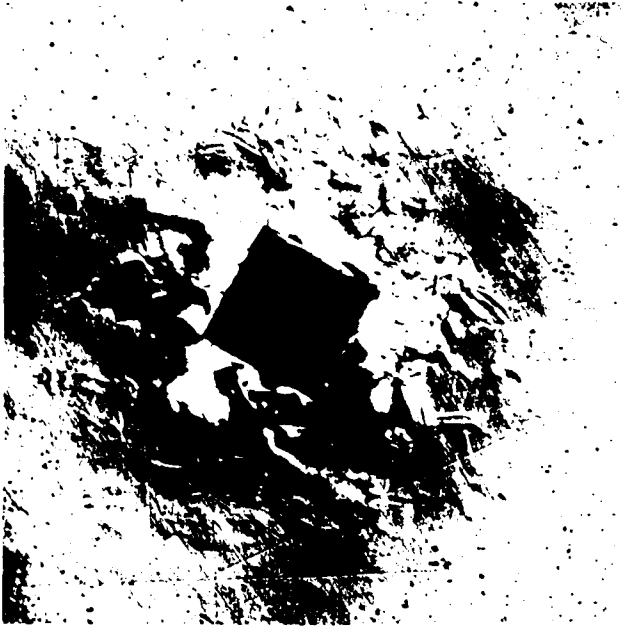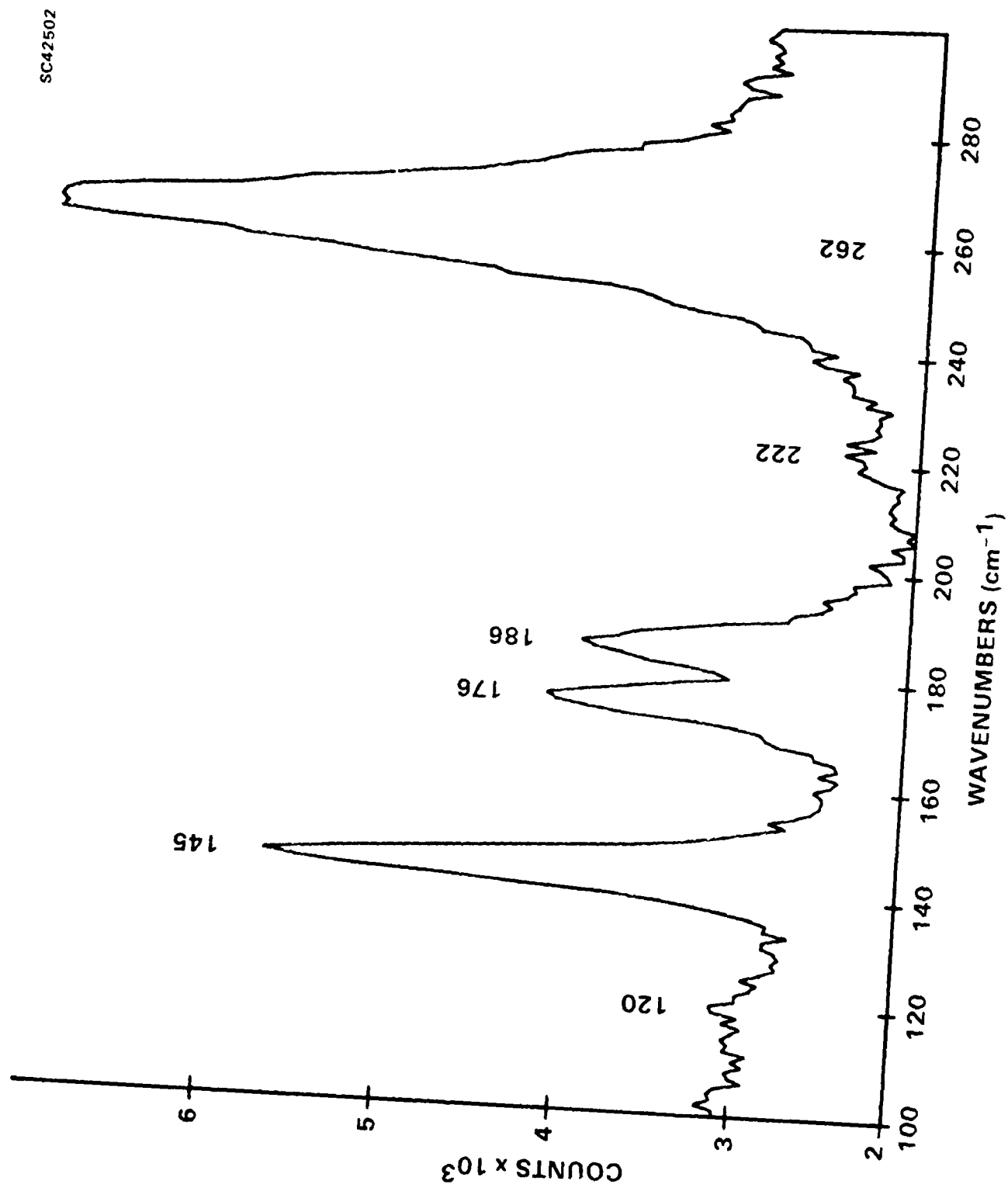
(A)

(B)

(C)

(D)

(E)

(F)

Figure 9A-F

(G)   (H)

Figure 9G,H

Figure 10

SC42502

37

Figure 11

38
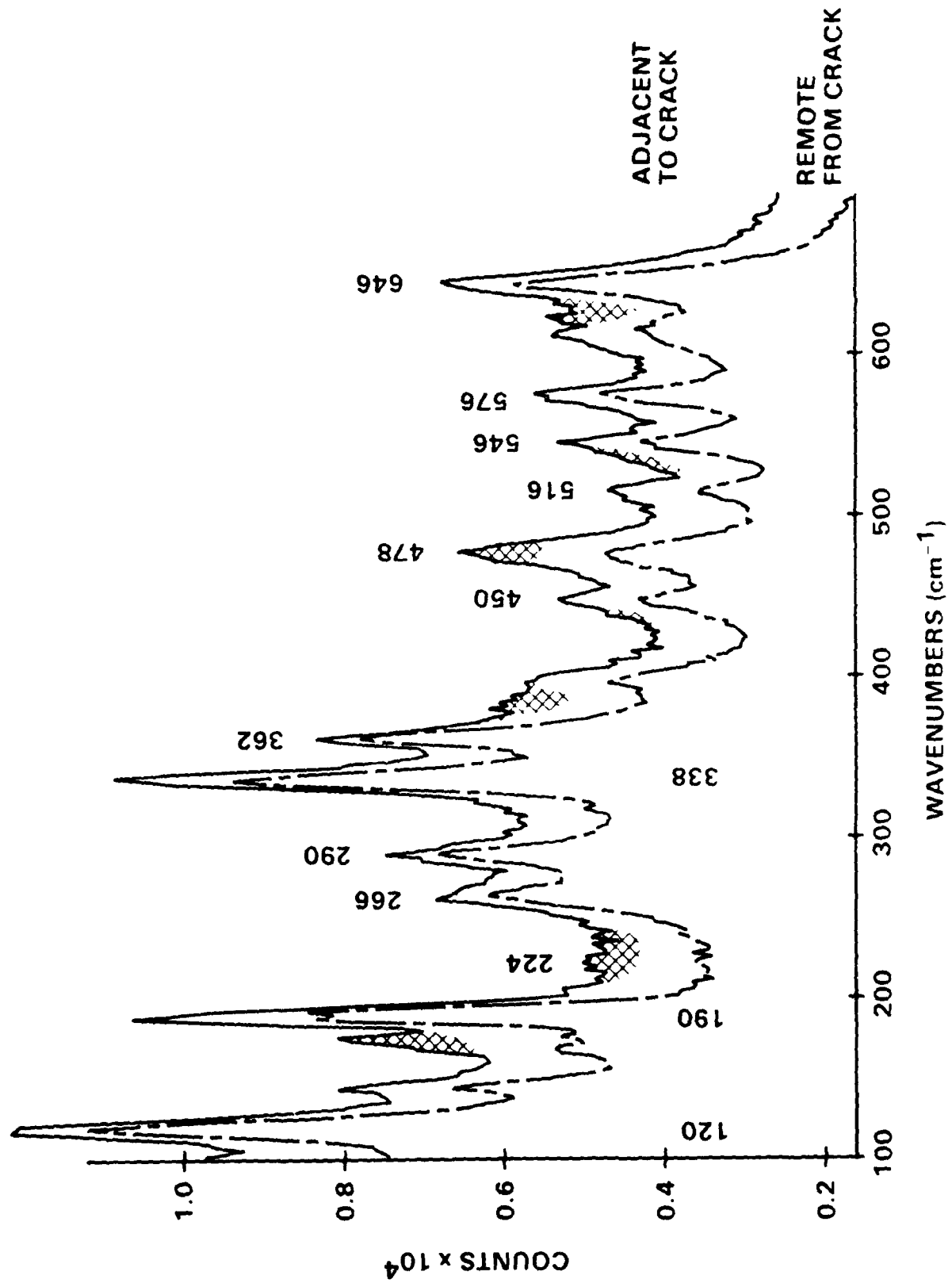
3. SURFACE DISPLACEMENT ANALYSIS OF THE TRANSFORMED ZONE
IN MAGNESIA PARTIALLY STABILIZED ZIRCONIA

SURFACE DISPLACEMENT ANALYSIS OF THE TRANSFORMED ZONE IN MAGNESIA PARTIALLY STABILIZED ZIRCONIA

B.N. Cox, Member of Technical Staff, D.B. Marshall, Manager, Ceramics Dept.
Rockwell International Science Center
Thousand Oaks, CA 91360

D. Kouris, Graduate Student and T. Mura, Professor
Dept. of Civil Engineering
Northwestern University
Evanston, IL 60201

ABSTRACT

The utility of surface displacement measurements as a source of quantitative information about subsurface plastic deformation is illustrated by analysis of the transformed zone in magnesia partially stabilized zirconia (Mg-PSZ). The surface displacements are derived from partial fringe analysis of optical interference micrographs. Their interpretation is based on analytical and numerical calculations of the surface displacements generated by a transforming semi-ellipsoidal inhomogeneity at the surface of a half-space. Inhomogeneous transformed zones, i.e., those possessing nonuniform distributions of transformation strain, are modeled as linear sums of nested, uniformly transforming semi-ellipsoids. It is found that the transformed zones around either through cracks or small, surface-breaking cracks in Mg-PSZ are indeed inhomogeneous. The degree of transformation is near the maximum possible only within a few microns of the crack plane. It falls away linearly or faster as the distance from the crack plane increases. Qualitative evidence suggests furthermore that significant net shear transformation persists near the crack plane. These conclusions are consistent with phase analysis using Raman spectroscopy.

1. INTRODUCTION

Advanced composites are finding ever increasing applications in the aerospace industry, in such systems as the Space Station, hypersonic vehicles, military aircraft, and space platforms. Many of these applications require materials that will survive in extreme environments (e.g., stress, high and low temperatures, radiation, and contamination) with stipulated service lives often measured in decades. Since such extreme conditions and long service histories are not always readily reproduced in the laboratory, accurate predictions of lifetime depend more heavily than ever before on understanding the mechanisms of degradation and failure on the most fundamental level possible.

In addition to the problems posed by the new levels of performance demanded of composites, modeling their properties and predicting their reliability are made even more challenging by the fact that they are themselves inherently complicated materials. They are generally constituted of two or more species of unequal elastic constants, plastic stress-strain responses, and coefficients of thermal expansion. They suffer highly inhomogeneous stress and strain fields when loaded either thermally or mechanically. Even at the outset of service, they contain large, inhomogeneous residual stresses generated during synthesis and processing by differential thermal expansion.

The characteristic length scale of the inhomogeneity of the stresses and strains is established by the geometry of the microstructure. For whisker-reinforced composites, it is tenths of microns to several microns; for fibrous composites it is 7-100 μm; for particulate-reinforced composites, 1-10 μm; and for transformation-toughened ceramics, 0.1-50 μm. Successful, fun-

damental research into the properties and reliability of composites therefore requires measurements of stresses and strains with submicron spatial resolution, and theoretical models that treat the material as discontinuous on the same microscopic scale.

The only current, quantitative experimental techniques possessing the required spatial resolution are those measuring surface displacements on external specimen surfaces. For submicron resolution, the most promising technique is measuring differential surface displacements by stereoscopy (e.g., Cox et al, 1986). Out-of-plane surface displacements can also be measured by interference microscopy, with transverse spatial resolution of 1-10 μm obtained from partial fringe analysis. Moire interferometry, x-ray analysis, and measurements of birefringence fail to meet the requirements of spatial resolution, and are not useful for all materials.

The fact that experimental data on the scale of the microstructure is restricted to surface displacements poses challenging theoretical problems. In general, the state of deformation in the bulk of a body cannot be uniquely determined from knowledge of surface displacements alone. Direct formulations of this problem are ill-posed, and have been solved successfully in limited cases only (Mura et al, 1986; Gao, 1987). However, progress can be made more generally if other information is available. The usual form of this information is subjective prejudice about the nature of the bulk deformation being determined, based on accumulated experimental evidence and the implications of theoretical models of the response of the material to external loads. When models are formulated that are admissible in light of such a priori information, quantitative information about bulk deformation can be deduced from surface displacements.

J8606D/sn

In this paper, the power of this approach will be illustrated by an analysis of the transformed zone in magnesia partially stabilized zirconia (Mg-PSZ). Mg-PSZ is representative of intrinsically brittle materials whose fracture toughness is enhanced by a stress-induced dilational phase transformation. When a crack forms in Mg-PSZ, the singular stress field triggers transformation of submicroscopic particles of the metastable tetragonal phase of $Mg-ZrO_2$ into the monoclinic phase. The phase transformation is accompanied by both a shear deformation and a volume dilation of ~ 4%. Since the transforming particles are confined to the environs of the crack in which the stress field is highest, i.e., to the transformed zone, a compressive residual stress forms at the crack tip and across the fracture surfaces. The effective stress intensity factor is reduced, R-curve behavior is observed, and toughnesses of ~ 18 MPA$\sqrt{m}$ have been achieved (Swain and Rose, 1986; Ready et al, 1987).

While the mechanics of toughening in transforming materials are understood in principle, the detailed characteristics of the transformed zone in Mg-PSZ are unknown. It is generally assumed for the purposes of theoretical modeling that the shear component of the transformation is nullified by multiple twinning within each transforming particle. There is micrographic evidence that this is approximately true around cracks, but not when transformation is induced by remote external loading in the absence of cracks (Marshall, 1987). It is also often assumed that the transformation is driven by some critical stress criterion, so that all particles within a certain boundary circumscribing a crack transform, and none beyond that boundary. This model implies a step function discontinuity in the magnitude of the net

transformation at the boundary of the transformed zone. Nonuniform distributions of transformation strain have been considered in theoretical models (Budiansky et al, 1983), but without direct experimental justification. In this paper, out-of-plane surface displacement measurements will be used to show that the transformed zone is indeed nonuniform, even well away from the zone's boundary. Qualitative evidence of significant net shear transformation will also be presented.

2. ANALYSIS OF TRANSFORMED ZONES IN Mg-PSZ

2.1   Theoretical Background

The surface displacements generated by a transformed zone are calculated by a combination of analytical and numerical procedures that promote efficiency and maximize simplicity. By following this path rather than using an FEM package, certain analytical properties of the displacements are exposed, and the task of interpreting experimental measurements is made much clearer.

Each transformed zone is considered to comprise a linear sum of nested, semi-ellipsoidal inclusions, each of which bears a uniform transformation strain (Eshelby, 1957) or eigenstrain (Mura, 1982). If the transformed zone is itself homogeneous, then a single semi-ellipsoidal inclusion is sufficient to model it. In any case, the basic problem from which any solution is constructed is that of a single, semi-ellipsoidal inclusion suffering a stress-free transformation strain, ε_{ij}^t, that defines the change in shape the inclusion would suffer in the absence of the constraining matrix. For the

transformed zone in Mg-PSZ, the inclusion can be taken to have approximately the same elastic constants as the matrix.

The surface displacements in such a system (Fig. 1) have been calculated and reported elsewhere for transformation strains whose principal axes coincide with the axes of the inclusion (Cox, 1987). Typical calculations of the normal component of displacement are shown in Fig. 2. For the present application, further important results are as follows.

1.   For plane strain conditions, i.e., the case of an inclusion for which $a/b \rightarrow \infty$, the normal component of displacement is given by

$$u_3(0,x_2,0) - u_3(0,0,0) = \frac{1-\nu}{2\pi} \left(-\sigma_3^{(1)}(0)\right) \left[(x_2-b)\ln\left|1-\frac{x_2}{b}\right|\right.$$

$$\left. - (x_2 + b)\ln\left|1 + \frac{x_2}{b}\right|\right] \quad , \qquad (1)$$

where ν is Poisson's ratio; and $\sigma_3^{(1)}(x_2)$ is the component of stress in the x_3 direction found for Eshelby's problem, viz., the case of a whole ellipsoid in an infinite medium. Equation (1) displays the expected logarithmic inflection at the boundary $x_2 = b$, and a flat plateau at $x_2 = 0$, similar to the curves of Fig. 2.

2.   For conditions only approximating plane strain, i.e., a/b large but finite, Eq. (1) remains an excellent approximation across any section of the inclusion, except in the far field ($x_2 \gg b$) or near the ends of the inclusion ($|x_1| \simeq a$).

3.   For $c \geq 3b$, further increases in the depth of the inclusion merely

raise the surface by a uniform amount over gauge lengths comparable

to the width 2b.

These results allow a computationally simple description of the

transformed zone in Mg-PSZ to be constructed, as described below.

2.2   Experimental Observations by Interference Microscopy

The normal component of the surface displacement around cracks in

specimens of Mg-PSZ was measured using interference microscopy. A typical

fringe pattern around the tip of a part-through crack is shown in Fig. 3.

Since the micrographs were exposed in green (thallium) light, successive

fringes delineate contours of elevation on the tilted specimen surface that

are separated by ~ 2700Å. Analyzing fractional fringe counts by eye and hand,

the normal displacement at any point can be determined to within ±200Å. The

displacements for the right-hand side of Fig. 3 are shown by the dashed curves

in Fig. 5.

Since the transformed zone is in compression, the fracture surfaces

of a crack in Mg-PSZ can be expected to be in contact unless there is an

external load or extreme fracture surface roughness. If the fracture surfaces

are in contact, and if the transformed zone accords with the common paradigm

of being essentially uniform, then the surface displacements should be similar

to those of Fig. 2. Comparison of Figs. 3 and 2 shows that this is not the

case. First, there is no inflection in the interference fringes to indicate a

well-defined boundary to the transformed zone. Second, nearly every fringe approaches the crack with cusp-like geometry. This second observation is true for every through crack and surface-breaking crack that has been examined. It cannot therefore be correlated with random crack openings in mode I or mode II, since it does not fluctuate with the stochastic microstructure. It apparently reflects a universal property of the transformed zone around all cracks in this material.

2.3   Model of an Inhomogeneous Transformed Zone

To model the experimental data successfully, it is necessary to consider transformed zones in which the transformation strain is nonuniform. This corresponds physically to having spatial variation in the fraction of tetragonal phase particles that have transformed to the monoclinic phase in the stress field of the crack. The analysis is simplified by fitting data some distance behind the crack tips, where the material is approximately in a state of plane strain, e.g., the displacements along the line AA' in Fig. 3. The inhomogeneous transformed zone is represented as the linear sum of nested semi-ellipsoids of large depth and infinite length along the direction of the crack. For either through cracks or surface-breaking cracks, the depth is much greater than the width of the zone. Thus, the surface displacements can be considered to be unaffected by the exact choice of depth, except for a uniform uplift. The uniform strain in each semi-ellipsoidal inclusion is assumed to be hydrostatic. If the nested semi-ellipsoids are labeled by the argument i, i = 1,...,N, then the transformation strain $\varepsilon^t(i)$ in the ith semi-ellipsoid is given by

$$\epsilon^t(i) = [\rho(b_i) - \rho(b_{i+1})] \cdot f \cdot \epsilon_0^t \qquad (2)$$

where b_i is the semi-axis of the ith semi-ellipsoid in the direction x_2; the density function $\rho(x_2)$ $(0 \leq \rho \leq 1)$ defines the fraction of tetragonal particles that have transformed; f is the volume fraction of the tetragonal particles; and ϵ_0^t is the linear dilational strain associated with the tetragonal to monoclinic transition. The normal displacement along the x_2 direction was calculated using the analytical result (Eq. (1)) for plane strain, summed over all the nested semi-ellipsoids. When the number of semi-ellipsoids is made large enough, a quasi-continuous variation of the density of transformation can be achieved.

ϵ_t^o was taken to be 0.013 and Poisson's ratio was taken to be either 0.2 or 0.3. The difference in the surface displacements calculated for these two values was nearly indiscernible, and had no effect on the results. A value $\nu = 0.23$ is reported for the material used by the manufacturer.* Young's modulus does not appear in the calculations.

Several parametric trial functions were tried for the fraction of transformed particles, $\rho(x_2)$. Four of the functions are displayed in Fig. 4. Calculated surface displacements were compared with those measured on various micrographs, and the parameters ρ_0 and x_0 in each trial function varied to optimize agreement. The curves shown in Fig. 4 correspond to the optimal values of ρ_0 and x_0 found by comparison with the data from Section AA' of Fig.

---

* Nilcra Ceramics (U.S.A.) Inc., St. Charles, Illinois

3. The corresponding surface displacements are compared with those data in Fig. 5. In each comparison in Fig. 5, the experimental and calculated displacements are set equal at x_2 = 50 μm, which turns out to be beyond the zone boundary.

It must be concluded from Fig. 5 and many similar comparisons that the fraction of transformed material within the transformed zone is nonuniform. The complete and nearly universal absence of any vestige of a plateau in the normal displacement at the crack implies that the density $\rho(x_2)$ falls away rapidly for $x_2 \geq 0$. The best agreement in Fig. 5 is obtained for the linearly decreasing trial function ρ_2 (Figs. 4b and 5b). The agreement obtained using the exponentially decaying function (Figs. 4c and 5c) or the cusped, circular function (Figs. 4d and 5d) is not much inferior. The optimized parameters for these three trial functions make them crudely equivalent. The best-fitted uniform distribution (Figs. 4a and 5a) produces displacements showing a clear plateau near the crack plane, in disagreement with the data.

In fact, the linear, exponential, and circular density functions also produce a slight plateau near the crack plane. With the provision that $\rho \leq 1$, no distribution of hydrostatic transformation was found that produced the cusp-like displacements found experimentally near the crack plane. This leads to the speculation that this feature of the data is attributable to net shear deformation on and near the crack plane.

3. DISCUSSION

The conclusion that the degree of transformation is approximately a linearly decreasing function of the distance from the crack plane can be tested qualitatively by phase analysis using Raman spectroscopy. Figure 6 indicates the fraction of monoclinic phase, the product of the toughening transformation, deduced from a scan by a Raman microprobe across the section AA' (Fig. 3) in the same Mg-PSZ specimen. The data in Fig. 6 show an estimate of the integrated strength of the signal from the monoclinic lines in the Raman spectrum relative to that from the tetragonal lines. Although it is difficult to assign absolute values to the volume fraction of the monoclinic phase, the trend revealed is in good agreement with the results of the surface displacement analysis. There is a background level indicated for the mono-clinic phase (the constant signal beyond ~ 50 μm in Fig. 6) corresponding to the concentration of that phase present in the material as prepared. When the background is subtracted out, the remaining signal corresponds to tetragonal phase transformed in monoclinic under the influence of the crack. Thus the intensity of the transformed material falls from its maximum to approximately zero in ~ 30 μm, in agreement with the optimized functions $\rho(x_2)$ of Fig. 4. Note that Raman spectroscopy is unable to distinguish the net shear deforma-tion, being sensitive only to the total amount of each phase and not to any twinning deformation.

The approach used in this paper of using trial functions to identify the spatial distribution of the transformation strain is effective, but not necessarily optimal. Its chief advantage is that is offers a controlled way of introducing physical intuition into the analysis of the surface displace-

ment data. The entire analysis was constrained to be consistent with certain physical limits: 1) that the transformation density ρ be bounded ($0 \leq \rho \leq 1$); 2) that ρ be a monotonically decreasing function of x_2; and 3) that ρ vanish beyond a finite interval of x_2, i.e., the transformed zone. It may well be that a less constrained method of deducing $\rho(x_2)$ would have worked equally well. For example, ρ could have been expanded as a linear sum of some basis functions, and the coefficients of the expansion determined by selecting the best fit to the data. This would have resulted in a system of linear algebraic equations, whose inversion would in principle give $\rho(x_2)$ directly. Whether such a formulation would be well posed requires investigation.

If the assumption of plane strain conditions is relaxed, the analysis of the data becomes more complicated, but by no means intractable. It is straightforward to apply the results of Cox (1987) to calculate surface displacements for a nested ensemble of semi-ellipsoids with any semi-axes a, b, and c. Physically reasonable ensembles can be invented readily to represent the crack-tip region, with a density function $\rho(x_1,x_2)$ analogous to that used here.

The method of analysis presented here and the results of Cox (1987) can be generalized easily to investigate transformations involving net shear as well as hydrostatic expansion. Such a generalization would allow quantitative testing of the conjecture that significant net shear exists near the crack plane. The same conjecture is also suggested by interference fringe micrographs of transformation not associated directly with cracks in Mg-PSZ, but occurring instead in bands confined to some grains in remotely loaded material. That the models assuming hydrostatic transformation failed to fit

the data exactly suggests that the data are sufficient to quantify the net shear strain.

CONCLUSIONS

1.   The usefulness of surface displacement measurements for revealing the nature of subsurface plastic deformation has been demonstrated by an analysis of the transformed zone around cracks in Mg-PSZ.

2.   The transformed zone has been shown to be nonuniform in the degree of transformation of the tetragonal phase particles. The degree of transformation falls away approximately linearly from the crack plane. There is qualitative evidence of significant net shear strain within a few microns of the crack plane.

REFERENCES

Budiansky, B., Hutchinson, J.W., and Lambropoulos, J.C., 1983, "Continuum Theory of Dilatant Transformation Toughening in Ceramics," Int. J. Solid Struct. 19, 337-52.

Cox, B.N., 1987, "Surface Displacements Generated by a Semi-Ellipsoidal Transformed Zone," submitted to J. Appl. Mech.

Cox, B.N., Morris, W.L., and James, M.R., 1986, "High Sensitivity, High Spatial Resolution Strain Measurements in Alloys and Composites," Proc. Conf. on Nondestructive Testing and Evaluation of Advanced Materials and Composites, Colorado Springs, CO, pp. 25-39.

Eshelby, J.D., 1957, "The Determination of the Elastic Field of an Ellipsoidal Inclusion and Related Problems," Proc. Roy. Soc. (London) 241A, 376-96.

Gao, Z., 1987, Dissertation, Northwestern University.

Marshall, D.B., 1987, unpublished work.

Mura, T., Cox, B., and Gao, Z., 1986, "Computer-Aided Nondestructive Measurements of Plastic Strains from Surface Displacements," Proc. Int. Conf. on Computational Mechanics, ed., S.N. Atluri, Springer-Verlag, Tokyo, pp. II43-II48.

Mura, T., 1982, "Micromechanics of Defects in Solids," Martinus Nijhoff, The Hague.

Ready, M.J., Heuer, A.H., and Steinbrech, R.W., 1987,. "On the Annealing of Test Specimens of High-Toughness Mg-PSZ," Submitted to J. Am. Ceram. Soc.

Swain, M.V. and Rose, L.R.F., 1986, "Strength Limitations of Transformation Toughened Zirconia Alloys," J. Am. Ceram. Soc. 69, 511-518.

FIGURE CAPTIONS

Fig. 1   An elemental semi-ellipsoidal transformed zone, showing its relation-
         ship to the coordinate system.

Fig. 2   Some calculations of the normal component of displacement, following
         Cox (1987). The cases shown are for uniform hydrostatic expansion of
         unit magnitude, (a) when $a/b = 1$ and (b) when $a/b = 10$. The normal
         component of displacement is plotted along the x_2-axis (Fig. 1). The
         circles in (a) show the values of x_2 at which calculations were made,
         the continuous curves being obtained by interpolation.

Fig. 3   Interference fringes around a surface-breaking crack in Mg-PSZ, the
         width of the field shown being 145 μm.

Fig. 4   Trial functions for the spatial variation of the fraction of
         transformed tetragonal particles.

Fig. 5   Comparison of the measured normal displacements along the line AA'
         (Fig. 3) with those calculated for the trial functions of Fig. 4.

Fig. 6   The strength of the Raman signal from the monoclinic phase peaks
         relative to that from the tetragonal phase peaks as a function of
         distance from the crack plane. The Raman scan was taken along the
         right half of the section AA' of Fig. 3.

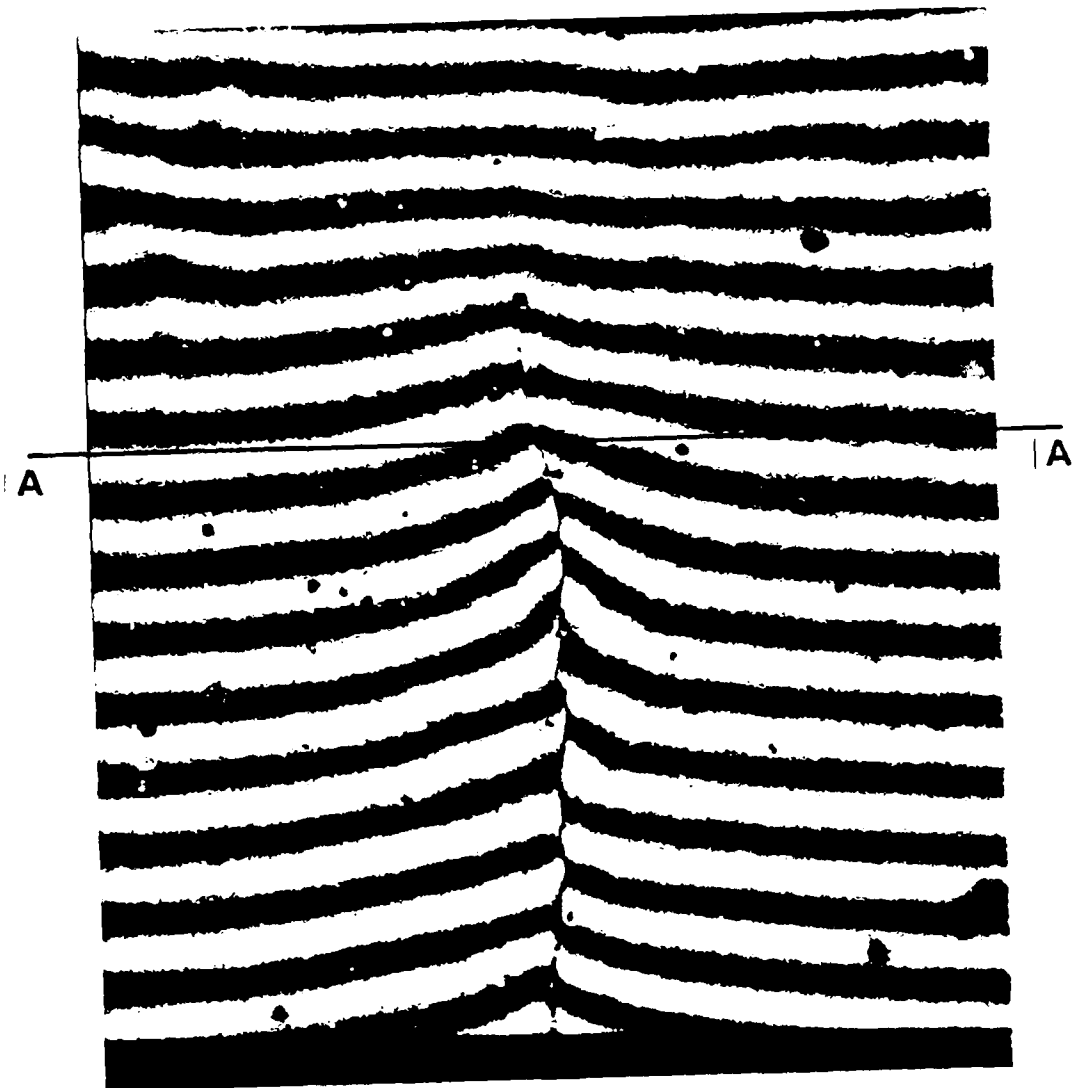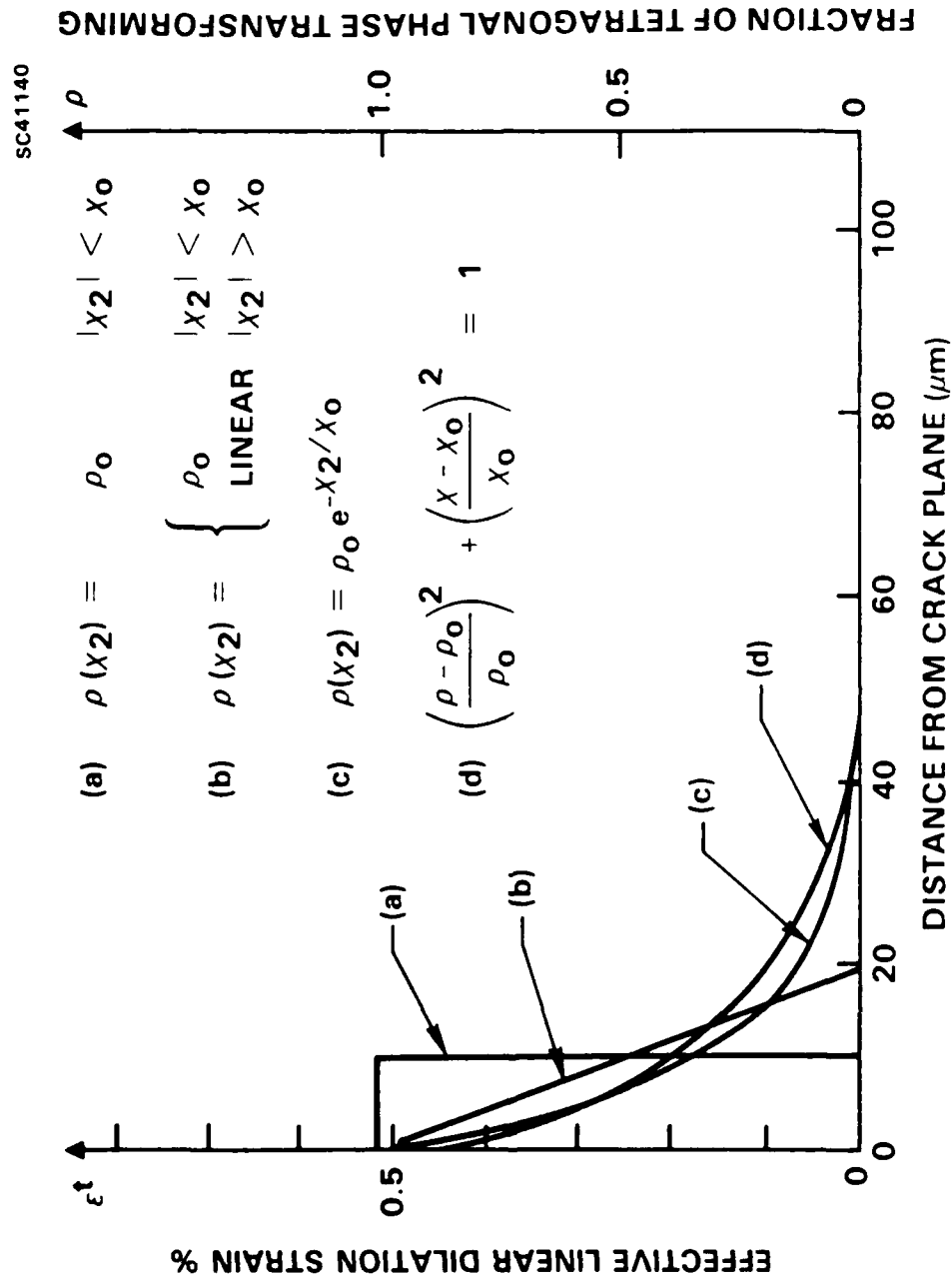SC39711
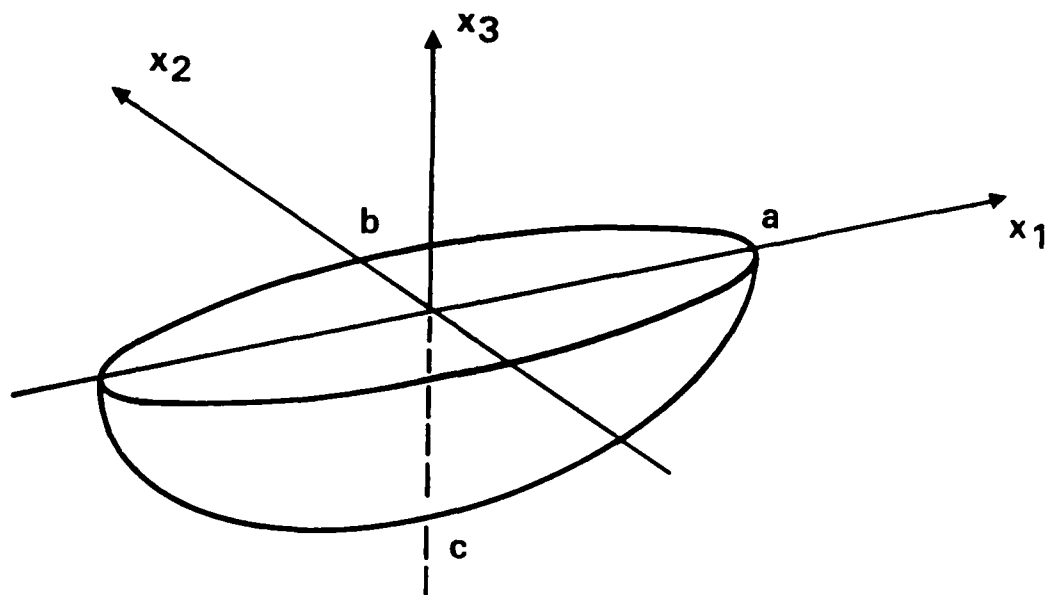
Figure 1
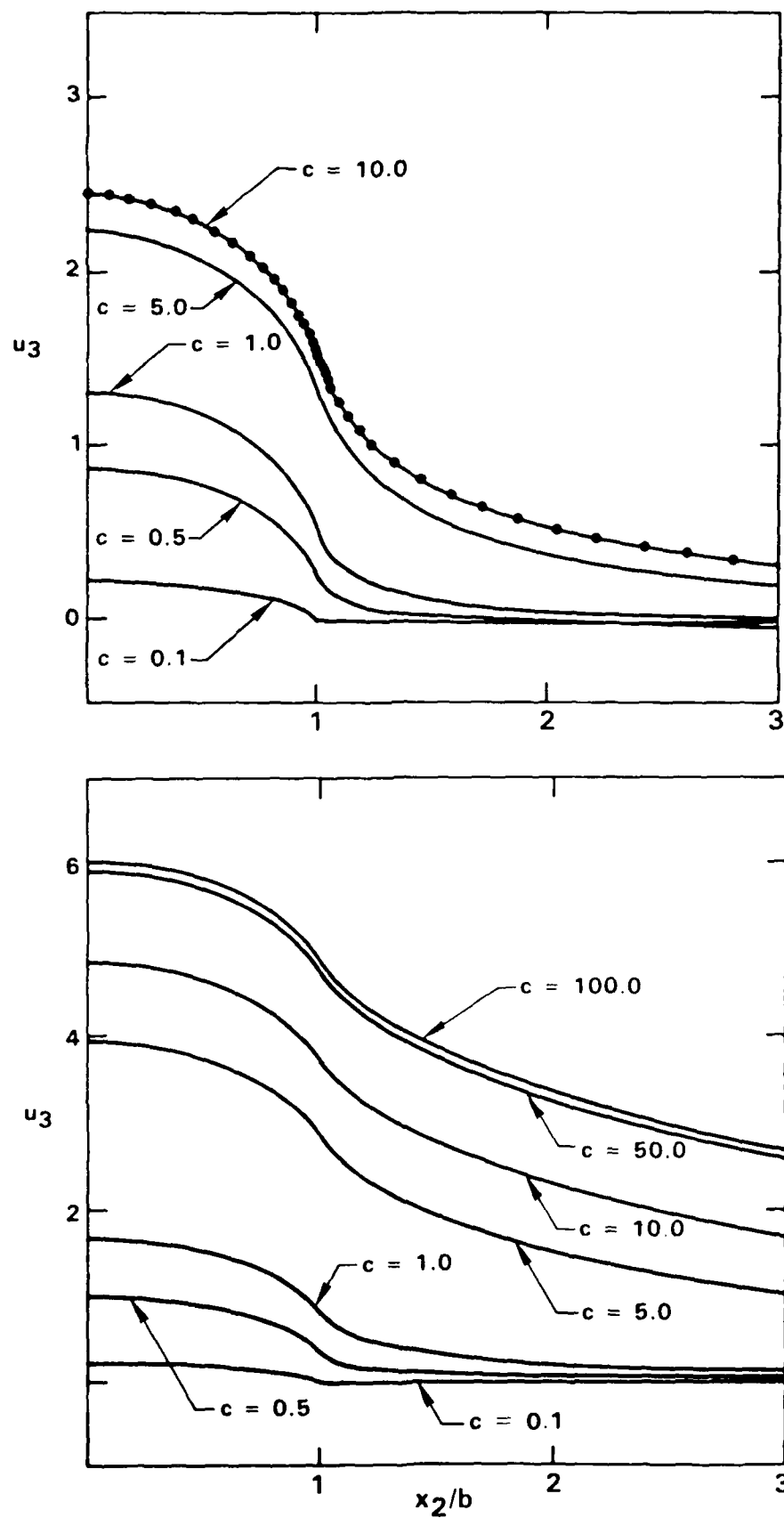
Figure 2

SC41068
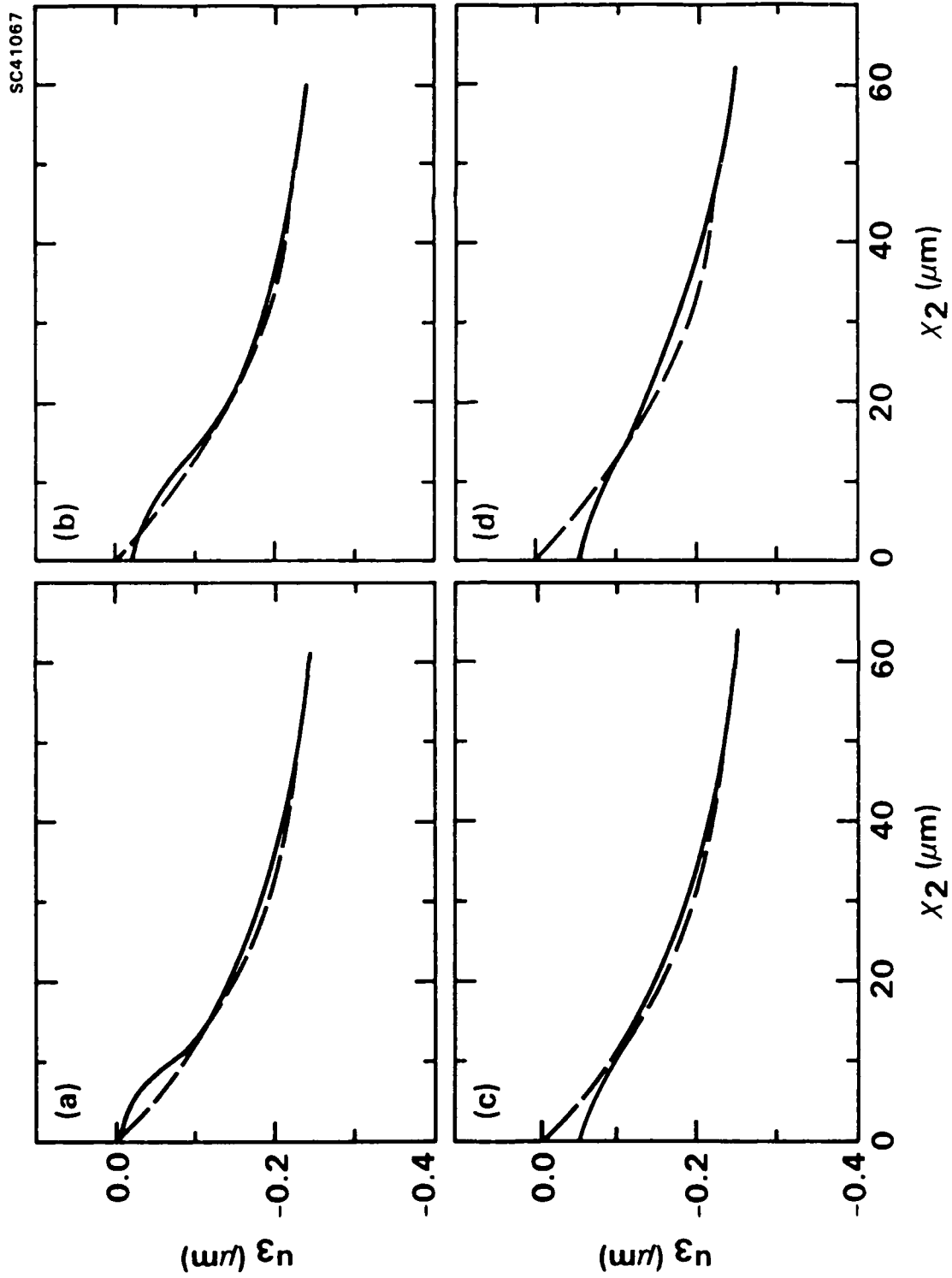
A |A′

Figure 3

FRACTION OF TETRAGONAL PHASE TRANSFORMING

SC41140

ρ

1.0

0.5

0

(a) $\quad \rho(x_2) = \rho_0 \qquad |x_2| < x_0$

(b) $\quad \rho(x_2) = \begin{cases} \rho_0 & |x_2| < x_0 \\ \text{LINEAR} & |x_2| > x_0 \end{cases}$

(c) $\quad \rho(x_2) = \rho_0 \, e^{-x_2/x_0}$

(d) $\quad \left(\dfrac{\rho - \rho_0}{\rho_0}\right)^2 + \left(\dfrac{x - x_0}{x_0}\right)^2 = 1$

100

80

60

40

20

0

DISTANCE FROM CRACK PLANE (μm)

Figure 4

(d)

(c)

(b)

(a)

ε^t

0.5

0.0

EFFECTIVE LINEAR DILATION STRAIN %

Figure 5

SC41067

59

SC41284
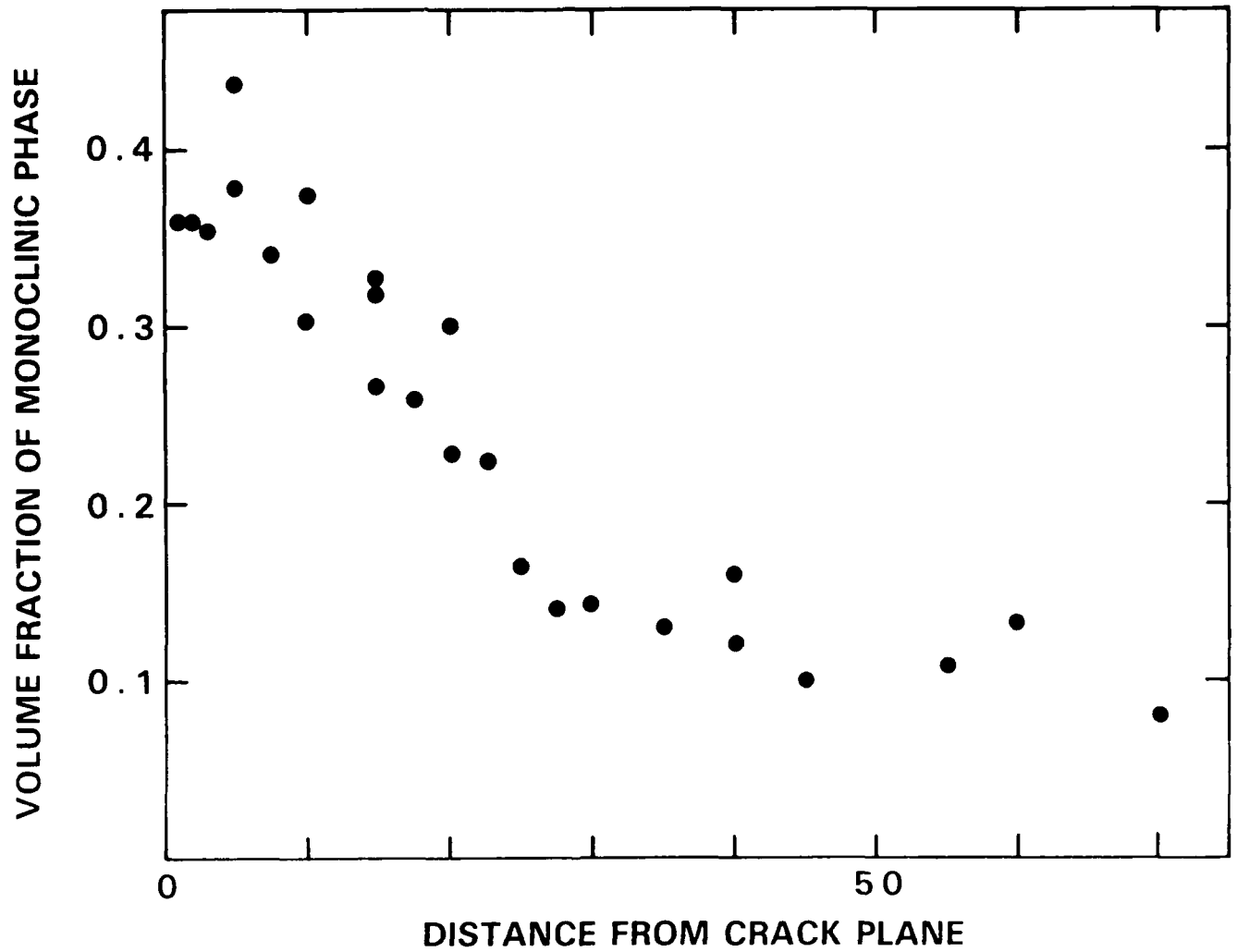
Figure 6

4. ON THE THERMOELASTIC MARTENSITIC TRANSFORMATION
IN TETRAGONAL ZrO$_2$

To be submitted to J. Am. Ceram. Soc.

ON THE THERMOELASTIC MARTENSITIC TRANSFORMATION IN TETRAGONAL ZrO$_2$

A.H. Heuer, M. Ruhle,* A.G. Evans* and D.B. Marshall**

Department of Metallurgy and Materials Science
Case Western Reserve University
Cleveland, OH 44106

and

*College of Engineering
University of California at Santa Barbara
Santa Barbara, CA 93106

and

**Rockwell International Science Center
Thousand Oaks, CA 91360

ABSTRACT

Recent evidence is summarized showing that the tetragonal (t) → monoclinic (m) transformation in ZrO$_2$ can occur <u>thermoelastically</u> in certain ZrO$_2$-containing ceramics, and that microcracking accompanying the transformation is more common than had previously been recognized. The implications of these new data for the size dependence of the transformation start (M$_s$) temperature and for the condition for stabilization of the stress-induced transformation product are discussed.

1. INTRODUCTION

Transformation toughening via the martensitic tetragonal (t) to monoclinic (m) transformation in ZrO_2 is one of the most effective ways of improving the reliability and structural integrity of engineering ceramics. The martensitic nature of the t → m transformation itself has not been an issue for a number of years,[1] but the crystallographic, thermodynamic and kinetic aspects of the transformation remain areas of considerable research interests[2-9] and even of some controversy.

One subject that is still not thoroughly understood is the particle size dependence of the "martensitic start" or M_s temperature. In the past, it has been argued that, like martensitic transformations in metallic systems, the martensitic transformation in ZrO_2 is nucleation-controlled.[6-8] Thus, the size dependence of the transformation temperature must be understood in relation to the effect of particle morphology (both size and shape) on the nucleation of the transformation, and possibly on the presence of defects to permit heterogeneous nucleation.[6-8] The notion of nucleation control appears to be widely shared,[4] although contrary opinions do exist.[11-13] One purpose of this paper is to reexamine the particle size dependence of M_s in the light of a variety of new data, in particular, the discoveries that (1) the transformation exhibits a degree of stress reversibility,[11-13] (2) that in some Mg-PSZs, an apparent general transformation of a fraction of t-ZrO_2 particles occurs under load prior to fracture and causes inelastic stress-strain curves and permanent deformation (~ 0.1% strain),[12,13] and (3) that micro-cracking associated with transformation is more common than has been previously appreciated.

2. REVERSIBLE TRANSFORMATION

Ma, McCartney and Ruhle[12] and Lee and Heuer[13] induced the t → m transformation in thin foils using stresses introduced by electron illumination in the transmission electron microscope (TEM). The work on Y_2O_3-containing t-ZrO_2 polycrystals (Y-TZP)[12] clearly shows (Fig. 1) that martensite laths nucleate at grain boundaries, presumably at sites where stress concentrations exist, and grow in apparent thermoelastic equilibrium across an individual grain in the fine-grained polycrystalline TEM foil. If a needle-like lath grows completely across a grain, it stops at a grain boundary and the resulting stress concentration at this site causes a differently oriented martensite lath to nucleate and begin to grow, sometimes back into the now partially transformed grain. If growth is controlled so that the lath extends only partly across a grain, e.g., by defocusing the electron beam to reduce the beam-induced stresses, the lath can shrink and leave a defect-free untransformed grain without any evidence that the grain had been partially transformed (Fig. 1d). In fact, on some occasions, when the specimen was further stressed by refocusing the electron beam, a differently oriented martensite lath formed, presumably because of differences in the biaxial stress distribution from one focusing experiment to the next.

A similar experiment was done by Lee and Heuer on a ternary Mg,Y-PSZ, in which the t-ZrO_2 precipitates were plate-like and could also be made to transform by beam-induced stresses. Strong autocatalytic transformation occurred in this alloy; when a single particle transformed the stress field so generated caused a neighboring particle to transform, until the entire illuminated region contained monoclinic (m) particles in the cubic (c) ZrO_2 matrix. The transformation occurred in a piece-wise fashion, with plate-shaped monoclinic variants forming on the c/t interface, growing into the precipitate, and then forming another variant, twin related to the first. Repeated growth by this

mechanism resulted in transversely twinned monoclinic precipitates. Partially transformed precipitates could be made to retransform to tetragonal structure by removing the electron beam, but if the entire precipitate transformed to monoclinic structure, the reverse transformation did not occur upon unloading.

X-ray evidence for a similar type of reversible t → m transformation under stress in bulk samples of Mg-PSZ has been obtained by Marshall and James,[11] who built a small bending fixture for mounting on an x-ray diffraction apparatus, mounted strain gauges on the samples, and loaded the samples to strains less than the fracture strain. The material had a background m-ZrO_2 content of approximately 13 vol%, but the m-ZrO_2 content could be reversibly increased (or decreased) by ~ 3 vol% by tensile loading (or unloading). When these same specimens were mounted on a loading stage on an optical microscope and viewed with a Nomarski interference objective, reversible surface roughness appeared on loading. The surface roughness was interpreted[11] as indicating the onset of the t → m transformation in favorably oriented grains; the scale of the surface roughness corresponded roughly with the grain size (~ 50 μm). Calculations showed that the magnitude of the surface distortions in these experiments was consistent with that expected from the transformation strain associated with the fraction of t → m transformation measured in the x-ray experiments.[11]

The surface roughening at various applied loads is shown in Fig. 2. The roughening was detectable by Nomarski interference at applied stresses above approximately 50 MPa and the magnitudes of the relative displacements increased continuously with increasing stress. The roughening was fully reversible provided the applied stress did not exceed 350 MPa. Moreover, from comparisons such as Figs. 2b and 2d, which show micrographs obtained at the same intermediate stress (100 MPa) during loading and unloading, no hysteresis could be detected during the reverse transformation. This obser-

vation suggests that the transformation occurs at, or close to, true thermoelastic equilibrium.

The reversible transformation in Mg-PSZ has also been observed in compressive loading. This is illustrated in Fig. 3, which shows the side surface of a beam loaded in four-point flexure (area between inner loading points). The applied stress increases linearly with distance from the center (neutral axis) of the beam, with the outer fiber stress being 300 MPa. Corresponding increases in surface distortions are evident in Fig. 3 on both the tensile and compressive sides of the beam. Moreover, the surface distortions appear to be of similar magnitudes on the compressive and tensile sides. These observations indicate that the reversible transformation is governed by the applied shear stress and is not sensitive to the hydrostatic stress component.

The specimen shown in Fig. 3 was unloaded after applying an outer fiber stress of 300 MPa and then reloaded with the sign of the bending reversed to allow direct comparison of transformation in a given area in tension and compression (Figs. 3b and 3c). By directly comparing areas that are uplifted and depressed in these micrographs, a one-to-one correlation is obtained showing a reversal of sign of surface distortion upon changing the applied stress from tension to compression (areas that are uplifted in tension are depressed in compression and vice-versa). This result is consistent with the transformation strains calculated assuming coupling of the strains and the applied shear stress (Appendix). These calculations indicate that in compressive loading the transformation always causes surface uplift, whereas in tensile loading the largest surface displacement is one of depression.

The Mg-PSZ material used to obtain Figs. 2 and 3 and in the work of Marshall and James contained a fraction of t-ZrO_2 precipitates that were so prone to transform

under stress that these specimens showed nonlinear stress-strain curves prior to fracture. This indication of transformation plasticity at a critical stress is similar to localized yielding in metals. The resulting fracture behavior of these specimens appears to be controlled by transformation plasticity, so that they exhibit R-curve behavior.[15,16] In such cases, the mechanical behavior is relatively insensitive to the presence of processing or machining flaws. Instead, failure is caused by microcracks that are generated by the transformation and grow stably during loading to sizes of the order of 0.5 mm.

Reversible surface transformation has also been observed in Mg-PSZ materials less prone to transformation, by Ready and Heuer[17] in a material that did not show inelastic yielding prior to fracture, but which did exhibit stable microcrack growth, and by Marshall and Swain[16] in a series of heat-treated materials with fracture toughnesses that ranged between $8 \, \text{MPa} \cdot \text{m}^{1/2}$ and $14 \, \text{MPa} \cdot \text{m}^{1/2}$. The lowest toughness material in this series exhibited neither inelastic yielding nor stable microcrack growth, whereas the highest toughness material showed both. The amount of reversible transformation at given applied stress did not vary within this series of materials with vastly different mechanical properties. Instead, an inverse correlation was found between the fracture toughness and the stress required to cause permanent transformation, indicating that it is the stabilization of the transformation that is the key to obtaining high toughness and damage tolerance.

3. IRREVERSIBLE TRANSFORMATION IN Mg-PSZ

Tensile loading of the high-toughness Mg-PSZ causes only reversible transformation provided the applied stress does not exceed ~ 350 MPa. At higher stresses, permanent transformation and microcracking develop (Fig. 4). The permanent transformation occurs in localized regions encompassing several grains; these regions are elongated on

the surface in the direction normal to the applied stress. Etching of the surface with HF reveals that these regions are composed of a substructure of well-defined, parallel-sided bands (Fig. 4b). Individual bands are confined to single grains, and the uplifted areas visible without etching contain arrays of adjacent grains with near-parallel bands. The surface traces of the bands are all oriented approximately normal to the applied stress.

Loading in compression also causes permanent transformation, but the stress required is considerably higher (1200 MPa) than in tension. Therefore, the critical stress to cause permanent transformation is strongly dependent on the hydrostatic stress component, in contrast to the response of the reversible transformation.

The development of permanent transformation in compressive loading can be seen in the series of micrographs in Fig. 5, taken at various stages during load/unload cycles (Fig. 5d). The surface roughening in Fig. 5a was similar to that in Fig. 2 and was reversible upon unloading. At increasing applied load (Fig. 5a to 5c), well-defined bands, with more severe surface uplift than that associated with the reversible transformation, developed within certain grains. With continued loading, individual bands increased in width and length, the number of bands within individual grains increased, and bands formed in new grains. Upon unloading (Figs. 5d and 5e), all of the transformation bands remained, but all of the other surface distortions disappeared.

The surface traces of the bands all lie at angles between ~ 30 and 90° to the direction of the applied stress (horizontal). Therefore, if these traces represent the intersections of the specimen surface with planar transformation bands, all of the bands could lie on planes of high resolved shear stress. The shear nature of these transformation bands is also suggested by the shape of the associated surface distortions. An optical interference micrograph from the area of Fig. 5f is shown in Fig. 6; the dark fringes

in this micrograph represent contours of constant height separated by $\lambda/2 = 2700\text{Å}$. The surface uplift along A-B is plotted in Fig. 6b. Within the bright bands in Fig. 5f, the surface is tilted at a constant angle, thus implying a large component of shear in the transformation strain.

A one-to-one correlation is evident in Figs. 5a through 5c between grains that were uplifted in Figs. 5a and grains that subsequently developed transformation bands in Figs. 5b and 5c. This observation establishes a direct connection between the reversible and permanent transformation.

4. MICROCRACKING AND TWINNING

A martensitic transformation proceeding in thermoelastic equilibrium generates very large residual stresses which oppose further transformation, and lead to reverse transformation on unloading. To prevent the reverse transformation, relief of these residual stresses must occur, for which twinning and microcracking are the likely mechanisms in ceramic matrices.

Microcracking has been observed around transformed $m\text{-}ZrO_2$ particles in the three types of transformation-toughened ZrO_2-containing ceramics now known. Examples are shown in Fig. 7; from ZrO_2-toughened Al_2O_3 in Fig. 8a, in Mg PSZ in Fig. 7b and 7c, and a Y-TZP example can be found in Fig. 7d. In ZTA, both tangential and radial (with respect to the Al_2O_3/ZrO_2 interface) microcracks can occur; the former are arrowed in Fig. 7a. Microcracks appear to be nucleated at the intersections of twin or variant boundaries with the Al_2O_3/ZrO_2 interface. Observations by several authors[18-20] suggest that tangential microcracking occurs if the thickness of individual twin plates exceeds ~ 50 nm and if no "domains of closure"[20] form.

Fu, Evans and Kriven[21] analyzed the stress distribution at the ends of such plates in particles in ZTA which consisted of two or six twins. Using linear elasticity, they found that for very small microcracks the stress intensity factor dropped below the critical stress intensity factor for crack growth, which had been estimated from experimentally determined crack arrest lengths. Thus, they concluded that spontaneous initiation of very small microcracks cannot be explained using linear elasticity and suggested that microcrack nucleation required the presence of lattice defects (e.g., dislocations), or involved nonlinear bond displacement in response to very high stress concentrations. High resolution TEM studies near crack tips by Wunderlich and Ruhle[22] eliminate the former model.

Figure 7b shows microcracks in a Mg-PSZ which has been heat treated so that the t-ZrO_2 particles, which are in poor contrast, are very prone to transform. The readily visible microcracks in the higher magnification region (Fig. 7c) formed during the accidental propagation of the microcrack seen in Fig. 7b. The last example is from Y-TZP (Fig. 7d). The overwhelming number of grains in this sample have tetragonal symmetry and contain 4.5 w/o $_2O_3$. However, the specimen had apparently been briefly heat treated in the two-phase (t-ZrO_2 + c-ZrO_2) phase field and formed some high solute content (~ 10.5 w/o Y_2O_3) c-ZrO_2 grains in equilibrium with some low solute content (~ 3.5 w/o Y_2O_3) t-ZrO_2 grains, whose M_s was above room temperature. Transformation in this material at M_s appeared always to cause microcracking of the type visible in Fig. 7d around the lowest Y_2O_3 content particles.

The transformation stresses that cause microcracking can be relaxed alternatively by formation of closure twins. These were first observed in ZrO_2-mullite materials,[23] and their role in stabilizing transformed particles was demonstrated recently in a ternary Mg, Y-PSZ alloy.[11] Transformation in this alloy proceeds by piecewise propa-

gation of twin-related variants along the initially tetragonal precipitates. Partial trans-formation occurs under thermoelastic equilibrium, but if an entire precipitate trans-forms, the transformed product becomes stabilized. Microcracking does not occur. Instead, the twin spacing at the end of a transformed precipitate is much finer than in the remainder of the precipitate (Fig. 8). Presumably, stress relief engendered by these closure twins prevents the reverse (m + T) transformation.

5. TRANSFORMATION REVERSIBILITY AND SIZE DEPENDENCE OF M_s

The in-situ transformation experiments (Figs. 1 and 2) clearly demonstrate that stress-induced reversibility in thin foils can arise from partial transformation and the same is assumed to be true in bulk specimens. The glissile nature of the martensitic interfaces between parent and product (t- and m-ZrO_2) is one of the hallmarks of martensitic transformations and this phenomenon is not surprising. These examples fur-ther show that partial, reversible transformation does not lead to any transformation debris. It is clear that the strains resulting from partial transformation cause stresses which oppose the applied stresses, leading to a state of thermoelastic equilibrium.

Two questions are posed immediately from the stress reversibility. The first is under what conditions is the t + m transformation in bulk specimens reversible on unload-ing, or to put it another way, under what conditions is it difficult to induce the reverse m + t transformation when a specimen is unloaded. The second question concerns the transformation thermodynamics and its relation to the observation of reversibility in the t + m transformation in bulk specimens, which suggests that a transformed m-ZrO_2 particle constrained by a matrix can have a higher free energy than an untransformed t-ZrO_2 particle in the same matrix.

5.1   Size Dependence of M_s

In the Marshall/James experiment, the matrix contained some stable m-ZrO_2 which transformed during cooling in the absence of any applied stress, and some t-ZrO_2 capable of reversible transformation. These observations may imply an intrinsic size dependence, as in fact was pointed out. However, rather than a surface energy argument for this size dependence of M_s, as suggested by Garvie and Swain,[9] we suggest that the difference may involve the effect of particle morphology on the strain energy arising from the transformation.

The elastic strain energy associated with a transformed inclusion is in general dependent upon its size and shape. For an oblate spheroid (axes a = b ≤ c) with unconstrained dilation and shear transformation strains e^T and e^T_{13}, the elastic strain energy in the matrix and inclusion after transformation can be expressed (from Eshelby[24])

$$E_T = E_0 + E_0 \frac{9\gamma (1-\nu)}{(1+\nu)} \left(\frac{e^T_{13}}{e^T}\right)^2 \tag{1}$$

where

$$E_0 = VE(e^T)^2/9(1-\nu) \quad , \tag{2}$$

V is the inclusion volume, E the Young's modulus (assumed equal for inclusion and matrix), ν the Poisson's ratio, and γ is a function of the aspect ratio a/c. The first term, E_0, in Eq. (1) is the contribution due to the dilation component of the transformation strain, and the second term arises from the shear component. The variation of E_T/E_0 with aspect ratio is shown in Fig. 9 for several values of the ratio e^T_{13}/e^T; $e^T_{13}/e^T = 0$ corresponds to pure dilational transformation (i.e., complete relief of shear strains by twinning), whereas $e^T_{13}/e^T = \frac{7}{4}$ corresponds to the unrelieved t → m transformation

strain in $ZrO_2(e_{13}^T \approx 0.07, e^T \approx 0.04)$. For pure dilation, the strain energy per unit volume is independent of inclusion shape, whereas the contribution due to the shear strain decreases with increasing aspect ratio. Since this elastic strain energy provides the resistance to transformation, and the chemical driving force per unit volume is independent of inclusion shape, the degree of undercooling needed for the transformation to become thermodynamically favorable decreases with increasing aspect ratio. Therefore, this effect could provide a rationale for an apparent size-dependent M_s if the precipitate aspect ratio increases with precipitate size. Observations of Farmer and Heuer are consistent with this hypothesis. They found that, in Mg-PSZ, $t-ZrO_2$ particles with aspect ratios ≤ 4 have M_s well below room temperature, those with aspect ratios between 4 and 5 still have $M_s <$ room temperature, but are sufficiently unstable that they often transform to an orthorhombic (o) form of ZrO_2 during TEM examination.* Specimens that were heat treated to encourage some precipitate growth have transformed particles with aspect ratios > 5.

5.2   Stabilization of the Stress-Induced Transformation Product

From the in-situ TEM observations (e.g., Fig. 1), it is clear that reversible transformation in Y-TZP and Mg,Y-PSZ involves reversible, stress-induced movement of the tetragonal/monoclinic interface. Stabilization of the monoclinic phase in these experiments was observed only when a lath grew completely across a grain in the Y-TZP, and when the precipitates in the Mg,Y-PSZ transformed completely. These observations are consistent with the notion that permanent transformation requires microcracking, or the formation of closure twins, as discussed in Section 4.

---

* This diffusionless t → o transformation at atmospheric pressure is believed to occur in TEM thin foil specimens;[26] no evidence for it has yet been found in bulk material.

Similar observations of partially transformed precipitates have not been made in Mg-PSZ. Therefore, experiments to date cannot distinguish whether the reversible transformation involves partial transformation of all precipitates or complete transformation of some individual precipitates. However, the direct connection between reversible and permanent transformation (Fig. 5) does confirm a previous suggestion that stabilization of the transformation requires a higher applied stress than does initiation of the forward transformation. Moreover, stabilization of the monoclinic phase in Mg-PSZ is always associated with bands that traverse grains, suggesting that precipitate interactions leading to strain localization are associated with the stabilization event, either as the cause or as a consequence.

If the reversible transformation in Mg-PSZ involves complete transformation of some individual precipitates, the observed continuous increase in surface distortions with increasing applied stress must be due to increasing numbers of transformed precipitates, according to a distribution of transformation stresses. In this case, stabilization would require irreversible, stress-relieving events to reduce the driving force for reverse transformation. This could be achieved by twinning and microcracking, both of which have been found by TEM to be ubiquitous at transformed precipitates in thin foils of this material (Section 4). However, a connection between this mechanism of stabilization and the formation of transformation bands is not evident. A more likely critical event for stabilization is the actual formation of a shear band of transformed precipitates (Fig. 10), which would lead to a reduction in the shear strain energy associated with each precipitate. Formation of the shear band requires interaction between precipitates and would be dictated by the statistical occurrence of a nucleus composed of a critical number of adjacent transformed precipitates. This mechanism does not preclude subsequent twinning and microcrack formation, and is therefore consistent with all of the observations.

If, instead, the reversibility involves partial transformation of many or all precipitates, with reversible movement of the tetragonal/monoclinic interface under an applied stress, then stabilization could also occur by microcracking or twinning. However, again, it is not evident why such a mechanism would lead to the bands of transformation observed in the experiments discussed in Section 3.

It is useful at this point to consider the thermodynamics of transformation. The total change in free energy ΔF of the system upon transformation of a volume V can be written[27-30]

$$\Delta F = -\Delta G + \Delta U_T - \Delta U_{int} + \Delta U_s \quad , \tag{3}$$

where ΔG is the decrease in chemical free energy, ΔU_T is the transformation strain energy, ΔU_{int} is the interaction energy for an applied stress σ_a, and ΔU_s is the change in surface energy (which may include strain energy associated with twin terminations at the precipitate boundary). The variation of the individual energy terms and the total energy with transformed volume, V, are shown schematically in Figs. 11a and 11b. If the shape of the transformed volume remains geometrically similar with increasing size, the first three terms in Eq. (1) are proportional to V, whereas ΔU_s is proportional to $V^{2/3}$, and a size effect exists (i.e., the energy change ΔF is negative for volumes larger than a critical value, V_c, and positive for $V < V_c$, Fig. 11b). This is the argument used by Garvie and Swain to explain the observed size effect in spontaneous transformation (i.e., in the M_s temperature). Alternatively, if the particle shape does not remain constant with increasing volume, the size effect is obtained without invoking the surface energy term because ΔU_T increases more slowly with increasing V, as discussed in Section 5.1. The requisite increasing aspect ratio with increasing transformed volume is exhibited by a growing lath as in Fig. 1, and by partly transformed precipitates as in Mg,Y-PSZ and Mg-PSZ.

In either case, the total energy change varies with volume and applied stress, as indicated in Fig. 11b. The energy ΔF^* in these plots represents a homogeneous nucleation barrier, and the curves predict complete transformation of precipitates with volumes larger than the critical value, V_c (V_c decreases with increasing applied stress), provided F^* is overcome. This is consistent with the response depicted in Fig. 10. However, stable movement of a transformation interface within a precipitate is not consistent with Fig. 11b. Such a response requires an additional energy term ΔU_c with the form represented in Fig. 11c, as would arise from an interaction strain energy with a localized stress concentration. In Mg-PSZ, stress concentrations have been observed at very small precipitates of Mg-rich δ-phase that form near the surfaces of the tetragonal precipitates.[29] It has also been suggested that stress concentrations occur at the edges of the precipitates because the profile is sharper than that of an oblate spheroid.[30] The total energy change in this case is shown schematically in Fig. 11d. Spontaneous transformation is predicted for volumes less than V_o. Moreover, V_o increases continuously (and reversibly) with applied stress as required for stable movement of the transformation interface. However, at the applied stress σ^* represented in Fig. 11d, the transformation extends indefinitely and irreversibly, thus defining the condition for permanent transformation. This description of the reversible transformation is simply the nucleation stage of transformation. For this mechanism to be consistent with the observations of Section 3, it would be necessary for the stress field surrounding the precipitate after unstable transformation to cause transformation at adjacent precipitates leading to the formation of a transformation band. Such autocatalytic transformation has been observed in in-situ experiments in Mg-Y-PSZ (Section 2), and is postulated to occur also in bulk Mg-PSZ.

APPENDIX

RELATIONS BETWEEN SURFACE DISTORTIONS AND TRANSFORMATION STRAINS

The surface distortions associated with the reversible transformation were of opposite sign in uniaxial tension and compression. This observation is consistent with a simple consideration of the transformation strains, assuming coupling of the strains to the applied shear stress. Each grain in Mg PSZ contains small, lens-shaped precipitates of tetragonal ZrO_2 in a solute-rich cubic matrix. The tetragonal c-axis of the precipitates is parallel to their smallest dimension. The precipitates are in three orientations, each with the tetragonal c-axis parallel to one of the cubic axes. If we assume a single lattice correspondence for the martensitic $t \rightarrow m$ transformation (e.g., lattice correspondence C for which the tetragonal c-axis becomes the monoclinic c-axis[31]), then an applied stress along a [110] cube direction (Fig. A1) provides the most favorable orientation for coupling with the shear strains. Then two sets of precipitates are oriented with Schmidt factors of 0.5 for (001)/[100] transformation shear, and the third set have zero shear stress on the (001) plane. In this orientation, transformation of equal numbers of the two sets of favorably oriented precipitates to single untwinned variants uniformly throughout the grain causes a total unconstrained strain of the grain

$$\epsilon_x = f(\pm \gamma/2 + e^T/3)$$

$$\epsilon_y = f(\mp \gamma/2 + e^T/3)$$

$$\epsilon_z = f e^T/3 \qquad \qquad (A1)$$

where the upper sign refers to tensile loading and the lower one to compressive, f is the volume fraction of the grain that transformed and γ and e^T are the unconstrained shear and dilation strains of the transformation (0.16 and 0.04, respectively[31,32]). The magnitudes of the strains for tension and compression are shown in Fig. A2.

Surface distortions arise from variations in the transverse strains, ϵ_y and ϵ_z, in adjacent grains. In compressive loading, both of the transverse strains are positive, indicating that the surfaces of transformed grains are always <u>uplifted</u>. In tensile loading, on the other hand, transformed grains can be either uplifted or depressed ($\epsilon_y < 0$, $\epsilon_z > 0$). However, the grains which experience the largest surface distortions (i.e., those oriented with ϵ_y normal to the specimen surface) are depressed in tensile loading and uplifted in compression, consistent with the observations of Section 3. Moreover, equal volume fractions of transformation in tension and compression (as would be implied by a critical shear stress criterion) would cause larger distortions in compression than in tension, as observed.

Relative axial and transverse transformation strains resulting from permanent transformation have been measured directly by Chen and Reyes-Morel[33] using strain gauges in uniaxial compression experiments. From the measured ratio of -2/3 (i.e., $2\epsilon_x/(\epsilon_y + \epsilon_z)$), the shear strain calculated from Eq. (A1) is $\gamma = (5/3)e^T \approx 0.07$. Therefore, as concluded by Chen,[33] ~ 50% of the available shear strain appeared in the macroscopic strain measurements in this case.

It is interesting to note that, for the volume fraction of reversible transformation in uniaxial tension measured previously using x-ray diffraction (~ 3%),[11] the magnitudes of the strains in the direction of the applied load ($\epsilon_x = -0.0018$ in compression and $\epsilon_x = +0.0027$ in tension) are similar (but of opposite sign) to the applied strain

($\sim \pm 0.0015$). This implies that in a fixed grips loading, the applied stress would be approximately relaxed by the transformation. Moreover, as shown previously,[11] the corresponding transverse strains $\epsilon_y \sim 0.002$ over a depth of about one grain diameter (~ 50 μm) would produce surface displacements ~ 100 nm, consistent with observations.

REFERENCES

1. G.M. Wolten, "Diffusionless Phase Transformation in Zirconia and Hafnia," J. Am. Ceram. Soc. 46 (9), 418-22 (1963).

2. E.C. Subbarao, M.S. Maiti and K.K. Srivastava, "Martensitic Transformation in Zirconia," Phys. Stat. Sol. A21, 9-40 (1974).

3. A.H. Heuer and L.W. Hobbs (eds), "Science and Technology of Zirconia," Advances in Ceramics, Vol. 3, The American Ceramic Society, Columbus, OH 1981.

4. N. Claussen, M. Ruhle and A.H. Heuer (eds), "Science and Technology of Zirconia II," Advances in Ceramics, Vol. 12, The American Ceramic Society, Columbus, OH 1984.

5. A.G. Evans and R.M. Cannon, "Toughening of Brittle Solids by Martensitic Transformations," Acta Met. 34 (5), 761-800 (1986).

6. I-Wei Chen and Y-H. Chiao, "Theory and Experiment of Martensitic Nucleation in ZrO_2-Containing Ceramics and Ferrous Alloys," Acta Met. 33 (10), 1827-45 (1985).

7. I-Wei Chen, Y-H. Chiao and K. Tsuzaki, "Statistics of Martensitic Nucleation," Acta Met. 33 (10), 1847-59 (1985).

8. A.H. Heuer and M. Ruhle, "On the Nucleation of the Martensitic Transformation in Zirconia (ZrO_2)," Acta Met. 33 (12), 2101-12 (1985).

9. R.C. Garvie and M.V. Swain, "Thermodynamics of the Tetragonal to Monoclinic Phase Transformation in Constrained Zirconia Microcrystals," J. Mat. Sci. 20, 1193-1200 (1985).

10. R.C. Garvie and M.F. Goss, "Intrinsic Size Dependence of the Phase Transformation Temperature in Zirconia Microcrystals," J. Mat. Sci. 21, 1253-57 (1986).

11. D.B. Marshall and M.R. James, "Reversible Stress-Induced Martensitic Transformation in ZrO_2," J. Am. Ceram. Soc. 69 (3), 215-217 (1986).

12. L. Ma, M.L. McCartney and M. Ruhle, to be published.

13. R.R. Lee and A.H. Heuer, "Thermoelastic Martensitic Transformation in (Mg,Y) PSZ," J. Am. Ceram.Soc., in press.

14. M.V. Swain, "Inelastic Deformation of Mg-PSZ and Its Significance for Strength-Toughness Relationships of Zirconia Toughened Ceramics," Acta Met. 33 (11), 2083-91 (1985).

15. D.B. Marshall, "Strength Characteristics of Transformation-Toughened Zirconia," J. Am. Ceram. Soc. 69 (3), 173-180 (1986).

16. D.B. Marshall and M.V. Swain, "Crack Growth Resistance in Magnesia-Partially Stabilized Zirconia," J. Am. Ceram. Soc., in press.

17. M.J. Ready and A.H. Heuer, to be published.

18. M. Ruhle, A. Strecker and D. Waidelich, "In-Situ Observations of Stress-Induced Phase Transition in ZrO_2-Containing Ceramics in Ref.4, pp. 256-282.

19. M. Ruhle, N. Claussen and A.H. Heuer, "Transformation and Microcrack Toughening as Complementary Processes in ZrO_2-Toughened Al_2O_3," J. Am. Ceram. Soc. 69 (3), 195-197 (1986).

20. M. Ruhle, to be published.

21. Y. Fu, A.G. Evans and W.M. Kriven, "Microcrack Nucleation in Ceramics Subject to a Phase Transformation," J. Am. Ceram. Soc. 9, 626 (1984).

22. W. Andersson and M. Ruhle, to be published.

23.

24. J.D. Eshelby, "The Determination of the Elastic Field of an Ellipsoidal Inclusion and Related Problems," Proc. Roy. Soc. 241A, 376 (1957).

25. S. Farmer and A.H. Heuer, to be published.

26. A.H. Heuer, L.H. Schoenlein and S. Farmer, "New Microstructural Features in Mg-PSZ," pp. 257-267 in Science of Ceramics 12 - Ceramurgica, s.r.l. Italy 1984.

27. A.G. Evans and A.H. Heuer, "Review-Transformation Toughening in Ceramics: Martensitic Transformation in Crack Tip Stress Fields," J. Am. Ceram. Soc. 63 (5-6), 241-248 (1980).

28. A.G. Evans, N. Burlingame, M. Drory and W.M. Kriven, "Martensitic Transformation in Zirconia - Particle Size Effects and Toughening," Acta Met. 29, 447-56 (1981).

29. F.F. Lange, "Transformation Toughening. Part I: Size Effects Associated with the Thermodynamics of Constrained Transformation," J. Mat. Sci. 17 (10), 225-234 (1982).

30. D.B. Marshall, A.G. Evans and M. Drory, "Transformation Toughening in Ceramics," in Fracture Mechanics of Ceramics, Vol. 6, pp. 289-307, ed., R.C. Bradt, A.G. Evans, D.P.H. Hasselman and F.F. Lange, Plenum, NY (1983).

31. W.M. Kriven, W.L. Fraser and S.W. Kennedy, "The Martensite Crystallography of Tetragonal Zirconia," pp. 82-97 in Ref. 3.

32. B.C. Muddle and R.H.J. Hannink, "Crystallography of the Tetragonal to Monoclinic Transformation in MgO-Partially Stabilized Zirconia," J. Am. Ceram. Soc. 69 (7), 547-55 (1986).

33. I-Wei Chen and P.E. Reyes Morel, "Implications of Transformation Plasticity in ZrO_2-Containing Ceramics: I. Shear and Dilation Effects," J. Am. Ceram. Soc. 69 (3), 181-9 (1986).

FIGURE CAPTIONS

Fig. 1   In-situ TEM observations of growth (A,B) and shrinkage (C,D) of a martensitic lath (monoclinic) in Y-TZP.

Fig. 2   Optical micrographs from tensile surface of flexure beam of transformation-toughened Mg-PSZ during load cycling. Nomarski interference used to highlight surface distortions. (A)-(C) increasing load: (A) zero, (B) 100 MPa, (C) 300 MPa. (D) and (E) unloading; (D) 100 MPa, (E) zero.

Fig. 3   (A) Optical micrograph from side of beam of Mg-PSZ loaded in four-point flexure (area between inner load lines), showing surface distortions on both the tensile and compressively loaded regions. Outer fiber stress 300 MPa. (B) Enlargement from (A) showing area from tensile side of beam. (C) Same area as (B), but after unloading and reloading with the sign of bending reversed to generate compressive stress. The Nomarski imaging conditions were identical for the micrographs of (B) and (C), giving the impression of low-angle illumination from the top right of the micrographs.

Fig. 4   (A) Polished surface of Mg-PSZ after applying tensile stress 420 MPa, showing uplifted regions due to permanent transformation. (B) Surface in (A) after etching for 4 min in HF, showing grain boundaries and transformation bands within individual grains.

Fig. 5   Optical micrographs, from the surface of a disc of Mg-PSZ that was loaded in diametral compression, during load cycling. The loading sequence and conditions under which the micrographs were obtained are indicated in (D).

Fig. 6   (A) Optical interference micrograph ($\lambda = 5400\text{Å}$) from area of Fig. 5(F) (Line X-Y corresponds to the same position in both); (B) surface uplift along x-y.

Fig. 7   Microcracking associated with transformed m-ZrO_2 particles in (A) ZTA, (B) and (C) Mg-PSZ and (D) Y-TZP.

Fig. 8   High resolution TEM image showing closure twins in (Mg,Y) PSZ. (Micrograph courtesy of R.R. Lee.)

Fig. 9   Plot of elastic strain energy in matrix and inclusion for an oblate spheroidal inclusion with aspect ratio a/c and unconstrained dilation and shear transformation strains e^T and e^T_{13}.

Fgi. 10   Schematic diagram illustrating reversible and irreversible transformation of precipitates in Mg-PSZ; (A) zero stress, (B) reversible transformation (isolated precipitates transformed), (C) permanent transformation (auto catalysis causes formation of transformation band).

Fig. 11   (A) Mechanism of reversible transformation by stress-induced movement of the tetragonal/monoclinic interface. (B) Variation of energy changes associated with tetragonal-to-monoclinic transformation in a constraining matrix with the volume transformed. (C) Change of total free energy of system with volume transformed. (D) and (E) energy changes in the presence of a localized stress concentration.

Fig. A1   Schematic diagram indicating transformation strains in tension and compression.

a

d

01μm

Figure

(A)

Figure 34

SC39424

(C)

(B)

Figure 3B, C

Figure 4

SC39426

(A) (B) (C)

(D) (E) (F)

100 μm

LOAD

TIME

A B C

E F

Figure 6

Figure 6

0.1μm

Figure 7R

93

Figure 7C

Figure 8

Figure 9

ISOLATED TRANSFORMATION
(REVERSIBLE)
(B)

TRANSFORMATION BAND
(IRREVERSIBLE)
(C)

(A)

SC39155

Rockwell International
Science Center

Figure 10

97

SC39157

(A)

Figure 11A

Figure 11B,C

Figure 11D,E

SC39153

100

Figure A1

5. CONTROLLING MICROSTRUCTURES THROUGH PHASE PARTITIONING FROM METASTABLE PROCESSES: THE ZrO_2-Y_2O_3 SYSTEM

To be published in Ceramic Ultrastructures, in press.

Controlling Microstructures Through Phase Partitioning From Metastable Precursors: the ZrO_2-Y_2O_3 System

F. F. Lange

Materials Department
College of Engineering
University of California, Santa Barbara
Santa Barbara, CA 93106

D. B. Marshall and J. R. Porter

Structural Ceramics Group
Rockwell Science Center
1049 Camino dos Rios
Thousand Oaks, CA 91360

1 Introduction

Transformation toughened materials fabricated in the ZrO_2-rich portion of the ZrO_2-Y_2O_3 system have received much attention since their introduction by Gupta and coworkers (1) (2). These materials are usually fabricated from powders made from a metastable precursor (eg, an aqueous solution $ZrClO_2$ and YCl_3) which is heat treated (calcined) at temperatures < 800°C to produce small crystallites (< 50nm). Figure 1 schematically illustrates the ZrO_2 rich portion of the ZrO_2-Y_2O_3 binary system. Transformation toughened materials fabricated in this system contain between 2 to 4 mole % (m/o) Y_2O_3 and are generally sintered at temperatures between 1300°C and 1600°C. The compositional boundaries of the two-phase, tetragonal (t) + cubic (c), field has been reported by several investigators who studied the ZrO_2 rich portion of the ZrO_2-Y_2O_3 system.

Scott (3) reported a eutectoid at 2.6 m/o Y_2O_3 and 565°C and indicated that both boundaries slightly curved towards lower Y_2O_3 contents with increasing temperature. Ruhle et al (4) analyzed different materials fabricated between 1300°C and 1600°C and reported similar boundary curvatures as indicated by Scott. Ruh et al, (5) report "......a two-phase .etragonal solid solution plus cubic solid solution exists from 1.5 to 7.5 [mole] % Y_2O_3 from 500 °C to 1600 °C." These boundaries would place the composition of all transformation toughened materials fabricated in this binary system in the two-phase field of the equilibrium diagram.

Experiments (1,6) show that the tetragonal structure (the toughening agent) is retained during cooling to room temperature if the grain size of the dense, polycrystalline material does not exceed a critical size (between 0.3 um and 1 um, depending on Y_2O_3 content). Theory suggests that the critical grain size is related to the thermodynamics of the tetragonal to monoclinic phase transformation as constrained by an elastic matrix. (6)

Recent observations (7) have shown that the grain size is very dependent on the Y_2O_3 content: at a processing temperature of 1400 °C, compositions within the apparent two phase region have grain sizes less than 1/5th those of compositions within the single phase tetragonal or cubic fields (0.3 um vs 2 um). It was hypothesized that the minor fraction of the expected second phase was hindering the growth of the major phase grains, eg, for compositions closer to the tetragonal phase field, smaller cubic grains were hindering the growth of the major phase tetragonal grains. However Heuer (8) pointed out that minor phase cubic grains are rarely smaller than the major phase tetragonal grains (a condition required for grain growth hindrance by a minor phase) in the materials he has examined. Therefore, a more extensive study was initiated to detail the microstructural development in the ZrO_2-rich portion (3 m/o Y_2O_3) of the ZrO_2-Y_2O_3 system. It will be shown that phase partitioning in this system is very sluggish and grains of a different crystalline symmetry need not be present to achieve fine grained material, despite the fact that such compositions are within a two phase region. Instead, adjacent tetragonal grains are observed to contain different amounts of Y_2O_3. These small non-equilibrium compositional differences from grain to grain are apparently developed by sluggish partitioning. Cubic grains are only observed after long partitioning periods. It is hypothesized that these differentials (or gradients) in yttrium content and the corresponding, differential lattice parameters are the cause for grain growth control. It is also observed that the ease of the stress induced tetragonal to monoclinic transformation, and thus, fracture toughness, is also governed by the sluggish phase partitioning, ie., the material becomes tougher with increasing heat treatment periods. Compositional changes induced by slow partitioning and changes in grain size also induced by heat treatment may concurrently control the fracture toughness of these important materials, but their independent effects on transformation can not be accessed with either previous or current data.

2 Experimental

For grain size and phase partitioning studies, aqueous solutions of zirconium acetate and yttrium nitrate of known equivalent concentrations of ZrO_2 and Y_2O_3, were mixed together to produce $Zr(Y)O_2$ solid-solution compositions containing between 0 and 3 m/o Y_2O_3 in increments of 0.25 m/o Y_2O_3. The solutions were evaporated to produce clear, glassy acetate granules, which were heated at 800 °C for 4hr and then heated to 1000 °C, 1200 °C, 1400 °C or 1600 °C at 5 °C/min and held for various periods and cooled at 20 °C/min. After heat-treatment, some of the sintered $Zr(Y)O_2$ granules where ground for phase analysis by XRD. The grain size on the as-sintered surfaces of the heat treated granules was determined by scanning electron microscopy (SEM) using the line intercept method. Other granules were embedded in epoxy and thinned both mechanically and by ion beam etching to produce specimens for observation in the transmission electron microscope (TEM) and the determination of yttrium distribution by energy-dispersive x-ray analysis.

For studies of the relation between microstructure and fracture toughness, commercial ZrO_2 powder (9) containing 3 m/o Y_2O_3 was colloidally treated to eliminate hard agglomerates and particles larger than 2 um (10). It was then consolidated in the slurry state by pressure filtration (11), dried, and sintered at 1400 °C/ 1h to produce a dense (relative density > 0.98) translucent disc. The disc was polished and then diamond cut into specimens suitable for phase determinations by XRD, indentation fracture toughness determinations (12), and grain size determination (thermal etching, SEM micrographs, line intercept method). Some specimens were subsequently heat treated at 1400 °C for various periods. A Raman microprobe (13) was used to determine the amount of transformed monoclinic ZrO_2 produced by the indentation as a function of distance from the indentation and heat treatment period. Known mixtures of monoclinic ZrO_2 (0 m/o Y_2O_3) and tetragonal $Zr(Y)O_2$ (3 m/o Y_2O_3) powders derived from the acetate precursors were used for calibration of the Raman microprobe measurements.

3 Results

3.1 Acetate Derived Materials

Heating the acetate derived materials at 600 °C for 16 h produced hard, black granules suggesting incomplete pyrolysis and the presence of carbon. Upon grinding and phase separation by a dispersion/sedimentation technique, a lighter colored powder could be separated from a black powder, suggesting that the carbon was a continuous phase in the partially sintered black granules. This is consistent with the observations of Leroy et al. who detailed the pyrolysis of Zr-acetate (14). Weight changes were not observed after 2h at 800 °C, suggesting pyrolysis was complete. Fully dense granules with grains that could be resolved with SEM (0.1 to 0.2 um) were produced after short periods at 1200 °C, suggesting that the grains grew at least one order of magnitude during pyrolysis, crystallization and densification.

3.1.1 X-ray Diffraction Analysis

For heat treatments at 800 °C/50hr all compositions had sharp diffraction peaks and exhibited only a tetragonal pattern for compositions containing $\geq$ 1 m/o Y_2O_3; whereas monoclinic ZrO_2 was a minor phase for compositions containing < 1 m/o Y_2O_3. At higher temperatures, the amount of monoclinic phase increased with heat treatment temperature and period, shifting the amount of Y_2O_3 required to prevent the tetragonal to monoclinic transformation during cooling to higher values. The tetragonal phase was not observed at room temperature after 200 hr at 1400 °C, and

50 hr at 1600 °C, ie, for these heat treatments, all tetragonal transformed to monoclinic during cooling.

Diffraction peaks clearly associated with cubic ZrO_2 were first discernible after 10 hrs. at 1400 °C. The amount of cubic phase increased with increasing heat treatment period at these two temperatures. After 200 hr at 1400 °C and 50 hr at 1600 °C, only monoclinic diffraction peaks were observed for compositions containing < 1.25 m/o Y_2O_3 and compositions containing ≥ 1.25 m/o Y_2O_3 were two phase, monoclinic and cubic ZrO_2. Figure 2 shows that the fraction of cubic phase increases with Y_2O_3 content for these heat treatments and suggests that 1.25 m/o is the solid solubility limit of Y_2O_3 in tetragonal ZrO_2 at these temperatures and heat treatment periods. Scott (15), who equilibrated compositions for 8 weeks at 1450 °C, suggests that the limiting solubility of Y_2O_3 in tetragonal is about 0.5 m/o Y_2O_3 relative to his previous result of approximately 2 m/o (3).

These data strongly suggest that phase partitioning is extremely sluggish and that the limiting solubility of Y_2O_3 in tetragonal ZrO_2 is much lower than initially suggested by Scott[3] and others.

3.1.2 Analytical Transmission Electron Microscopy

Figure 3 shows distributions of yttrium contents within individual grains in specimens with an overall composition of 2.25 m/o Y_2O_3 (4.34 w/o yttrium) heat treated at 1400 °C for 1 hr and 50 hrs. Because the grains within each grouping were individually analyzed without tilting the foil between observations and without precluding occasional through thickness, overlapping grains, the analysis obtained from some 'single' grains were an average of two.

Only tetragonal grains were observed for the 1 hr heat treatment and, as shown in Fig 3, each grain had a slightly different Y_2O_3 content than its neighbors. Monoclinic, tetragonal and cubic grains were observed in the specimen that had been heat treated for 50 hrs. The cubic grains were always smaller than their neighboring monoclinic or tetragonal grains and contained 12.7 w/o yttrium (6.6 m/o Y_2O_3). Consistent with XRD results, these data show that equilibrium phase partitioning was not observed in the material heat treated for only one hour, whereas some equilibrium partitioning did occur after 50 hrs.

3.1.3 Grain Size

Figure 4 illustrates the grain size vs Y_2O_3 content for different heat treatment periods at 1400 °C and 1600 °C. Data were not obtained at 1600 °C for compositions containing < 0.5 m/o Y_2O_3. Consistent with previous data obtained from materials processed from commercial powders (7), the grain size decreased with increasing Y_2O_3 content. Grain growth is extremely sluggish for compositions containing Y_2O_3 relative to the rapid growth observed for the 'pure' ZrO_2.

Bimodal grain size distributions (indicative of abnormal grain growth) were only observed for compositions containing < 0.5 m/o Y_2O_3 heat treated at 1400 °C for 0 h. When these materials were heat treated for 1 h, the average grain size was approximately that of the larger grains observed in the bimodal distribution. For all other compositions and heat treatment conditions, the ratio of the largest grain observed to the average size was ≤ 2.5, ie, indicative of normal grain growth.

3.2 Material Sintered from Powder Containing 3 m/o Y_2O_3

3.2.1 Phases and Grain Size

Figure 5 illustrates the grain size as a function of the heat treat period at the temperature (1400 °C) used to sinter the material initially. The grain sizes are nearly identical to those obtained from the acetate derived material containing the same Y_2O_3 content. As shown in this figure, diffraction peaks attributed to cubic and monoclinic ZrO_2 were first observed after periods of 20 h and 120 h, respectively.

3.2.1 Fracture Toughness

Figure 6 illustrates the fracture toughness as a function of heat treatment period at 1400 °C. For periods > 30 h, scatter due to variable crack lengths from the corners of the vickers indenter became significant. Although it is questionable whether the fracture toughness calculated from indentation measurements are valid for transformation toughened materials (residual stress field due to transformed material around the indentation provides an additional driving force for crack extension) the data show that the resistance of the material to crack extension increases with heat treatment period. During this heat treatment period, the hardness decreased from 14.3 GPa to 12.7 GPa. It should be noted that no monoclinic ZrO_2 was observed on the heat treated surfaces by XRD prior to the indentation measurements.

Figure 7 shows the results of the raman microprobe analysis reported as the calibrated volume fraction of retained tetragonal ZrO_2 as a function of distance (perpendicular) from the edge of the indentation. As shown, the amount of material transformed due to the indentation stress field increased with heat treatment period. These results show that the tetragonal material becomes easier to transform with increasing heat treatment period, consistent with the toughness data in Fig. 6.

4 Discussion

Data for both the acetate and powder derived materials show that the partitioning kinetics are extremely sluggish. Since the powder was manufactured (9) by mixing solutions of $ZrOCl_2$ and YCl_3, hydrolyzing, drying and calcining at temperatures below 1000 °C, one would expect that these powders are as much of a metastable precursor as the acetate derived material and that sintering at 1400 °C for several hours would do little in producing an equilibrium phase assemblage.

It was previously suggested (6) that retention of the tetragonal structure in this compositional system by elastic constraint is directly associated with grain size. It is now clear that concurrent effects due to partitioning (ie, redistribution of composition) and grain size would be difficult to separate in any previous experiment. That is, the ease in which the tetragonal phase transforms to the monoclinic structure either during cooling from its fabrication temperature, or when acted upon by the stress field of a crack, will depend on its Y_2O_3 content. As partitioning proceeds, the Y_2O_3 content of the tetragonal phase decreases towards its equilibrium value as the Y_2O_3 rich cubic phase grows. The ease of the transformation will therefore increase as the Y_2O_3 content in the tetragonal phase diminishes during sluggish partitioning. Grain growth is concurrent with partitioning, and its separate effect on the retention of the tetragonal structure will be difficult to ascertain. It might be concluded that all transformation toughened materials fabricated in this system are not equilibrium compositions.

4.1 Grain Growth

The question of why grain growth is so inhibited in this system still remains. A second phase (eg, smaller cubic grains) is not observed during initial heat treatment periods and therefore can not be the reason for grain growth inhibition as initially suggested (7). Instead, we observe that each grain has a slightly different yttrium content than its neighbors. Smaller cubic grains only develop after an extended period of partitioning. Based on these observations, one might hypothesize that compositional differences from grain to grain and compositional gradients within grains are responsible for grain growth inhibition, and may contribute to the slow partitioning kinetics..

As reported by Scott (3) the lattice parameters of tetragonal ZrO_2 depend on composition (yttrium content). As recently proposed (16), if adjacent grains have the same structure, but different composition, any grain boundary movement without compositional adjustment would produce a plane of structural discontinuity, ie., a coherent interface within the growing grain with a strain energy related to the differential lattice parameters. The strain energy per unit volume associated with the coherent interface produced by grain boundary motion is a retarding 'force' and thus reduces the driving 'force' for grain boundary motion. As grains become larger, the radius of curvature of their boundaries become larger, which reduces their driving 'force' for motion. Analogous to the concept introduced by Zener (17) for grain growth hindrance by particulates, when the driving 'force' becomes equal to the retarding 'force', grain growth will stop. This concept is consistent with observations. That is, during and after densification, the ZrO_2 crystallites grow by at least an order of magnitude within a relatively short period (ie, within the 1 to 2 hours it takes to heat the material to 1400 °C). Further grain growth for compositions within the two phase field, requires extended heat treatment periods.

4.2 Partitioning

During pyrolysis, the acetate derived compositions with Y_2O_3 contents between 1 and 3 m/o crystallize with the tetragonal structure as observed in this study after cooling from 800 °C (Leroy et al. who detailed the crystallization between 250 °C and 750 °C, suggests that 'pure' ZrO_2 does the same). Partitioning, which requires the diffusion of Y^{+3} (the counter diffusion of Zr^{+4} and O^{-2} is implied throughout) occurs over long periods at high temperatures. Figure 8 schematically illustrates the free energy functions at a given temperature for the tetragonal and cubic structures of ZrO_2 as a function of composition (Y_2O_3 content). The common tangent to both functions defines the equilibrium composition of each structure; ΔG_p^o is the chemical free energy change driving partitioning for the metastable tetragonal composition defined by the broken line. $\Delta G_p^o \rightarrow 0$ as the initial composition approaches the equilibrium composition of the tetragonal structure.

Partitioning requires the nucleation and growth of a volume element (precipitate or grain) with the equilibrium composition of the cubic structure. (Nuclei may already exist if a powder contains Y_2O_3-rich particles; these particles would grow into large cubic grains during partitioning.) Yttrium must diffuse to these growing cubic volume elements, which are expected to nucleate at 4-grain junctions, ie, sites of lowest free energy. If it is assumed that grain boundary diffusion is much faster than volume diffusion, yttrium within the metastable tetragonal grains will slowly diffuse to the closest grain junction and then rapidly to the growing cubic grain. The yttrium content of the material adjacent to these grain junctions will be less than that within the grain, ie, grain junction compositions will attempt to approach the equilibrium composition of the tetragonal structure. Compositional gradients will arise between the interior of grains and their junctions. Because lattice parameters are dependent on composition, compositional gradients will give rise to strain energy, which in turn, will decrease the driving force for partitioning.

5 Concluding Remarks

Phase partitioning in the ZrO_2-Y_2O_3 system was observed to be extremely sluggish and may require many weeks at usual sintering temperatures to establish equilibrium phases. The composition of tetragonal grains within transformation toughened materials fabricated in this system will be metastable. Partitioning occurring during extended heat treatments at high temperatures will cause the tetragonal grains to approach their equilibrium composition, making them more susceptible to transformation either during cooling or when acted upon by a stress field. The equilibrium Y_2O_3 content of the tetragonal phase may be as low as 0.5 m/o at sintering temperatures as suggested by Scott (15) for heat treatment periods of 8 weeks. Our data, obtained for relatively short heat treatment periods (200 h), indicates a value < 1.25 m/o.

Grain growth in dense materials fabricated in the two phase field is also extremely sluggish, but can not be correlated to the hindrance of grain boundary motion by cubic grains. Instead, it is hypothesized that boundary motion is hindered by compositional differences between grains, developed during partitioning. It is also hypothesized that compositional gradients will arise between grain interiors and their junctions during partitioning. Because the lattice constants of tetragonal ZrO_2 vary with composition, compositional differences and gradients will produce strain energy which will hinder both grain growth and partitioning.

Rockwell International
Science Center
8

Acknowledgement

References

1) T. K. Gupta, F. F. Lange and J. H. Bectold, "Effect of Stress Induced Phase Transformation on the Properties of Polycrystalline Zirconia Containing Tetragonal Phase," J. Mat. Sci. 13, 1464 (1978)

2) T. K. Gupta, J. H. Bechtold, R. C. Kuznicki, L. H. Cadoff, and B. R. Rossing, "Stabilization of Tetragonal Phase in Polycrystalline Zirconia," J. Mat. Sci. 12, 2421 (1977).

3) H. G. Scott,"Phase Relationships in the Zirconia-Yttria System," J. Mat. Sci. 10, 1527 (1975).

4) M. Ruhle, N. Claussen and A. H. Heuer, "Microstructural Studies of Y_2O_3-Containing Tetragonal ZrO_2 Polycrystals (Y-TZP)," Advances in Ceramics, Vol 12, Science and Technology of Zirconia II, ed by Nils Claussen, Manfred Ruhle, and Arthur H Heuer, p352, American Cermic Society, Columbus, Ohio (1984).

5) R. Rühle, K. S. Mazdiyasni, P. G. Valentine and H. O. Bielstein, "Phase Relatons in the System ZrO2-Y2O3 at Low Y2O3 Contents," ibid, 67, C-190 (1984).

6) F. F. Lange, "Transformation Toughening: Part I, Size Effects Associated with the Thermodynamics of Constrained Transformations," J. Mat. Sci. 17, 225-34 (1982).

7) F. F. Lange, "Transformation-Toughened ZrO_2: Correlations Between Grain Size Control and Composition in the System ZrO_2-Y_2O_3," J. Am. Ceram. Soc. 69 [3] 240-2 (1986).

8) A. Heuer, private communication

9) Toyo Soda Manufacturing Co. ,Tech. Bul. No. Z-051, Japan

10) F. F. Lange, B. I. Davis, and E. Wright, "Processing-Related Fracture Origins: IV, Elimination of Voids Produced by Organic Inclusions," J. Am. Ceram. Soc. 69 [1] 66-9 (1986).

11) F. F. Lange and K. T. Miller, "Pressure Filtration: Kinetics and Mechanics," To be published

12) G. R. Anstis, P. Chantikul, B. R. Lawn and D. B. Marshall, "A Critical Evaluation of Indentation Techniques for Measuring Fracture Toughness: I Direct Crack Measurements Strength Method," J. Am. Ceram. Soc. 64 [9], 533-8 (1981).

13) D. R. Clarke and F. Adar, "Measurement of the Crystallographicaly Transformed Zone Produced by Fracture in Ceramics Containing Tetragonal ZrO_2 '" J. Am. Ceram. Soc. 65 [6] 284-88 (1982).

14) E. Leroy, C. Robin-Brosse and T. P. Torre, "Fabrication of Zirconia Fibers from Sol Gels," in UltraStructures Processing of Ceramics, Glasses, and Composites, Ed. by L. L. Hench and D. R. Ulrich, pp. 219-31, Wiley & Sons, New York,1984.

15) H. G. Scott, "Phase Relationships in the Magnesia-Yttria-Zirconia System," J. Aust. Ceram. Soc. 17 [1],16-20 (1981).

16) F. F. Lange, "Controlling Grain Growth," Proc. 3rd Microstructure Conf on Ceramics, Aug. 1986, Berkeley.

17) C. Zener, kindly quoted by C. S. Smith, Trans. Met. Soc. AIME, 175, 15 (1949).

Figure Captions

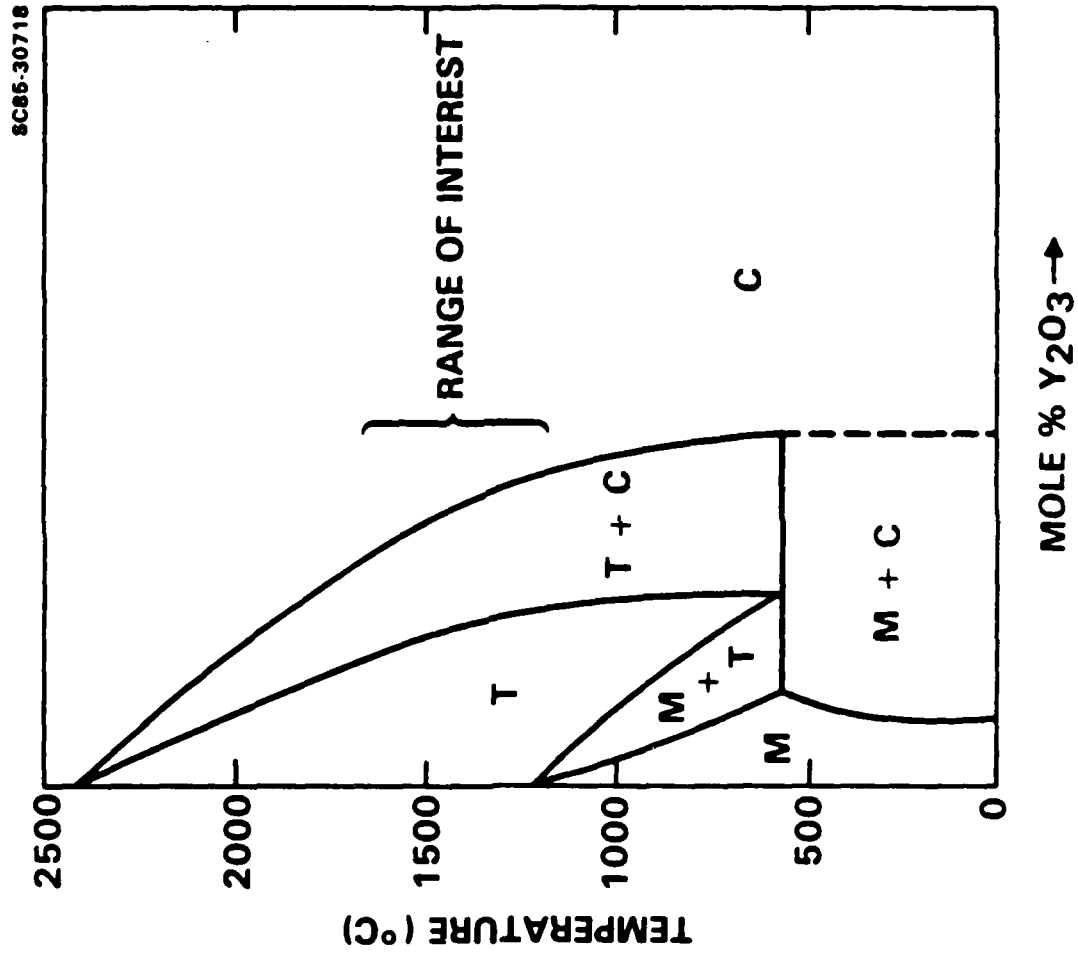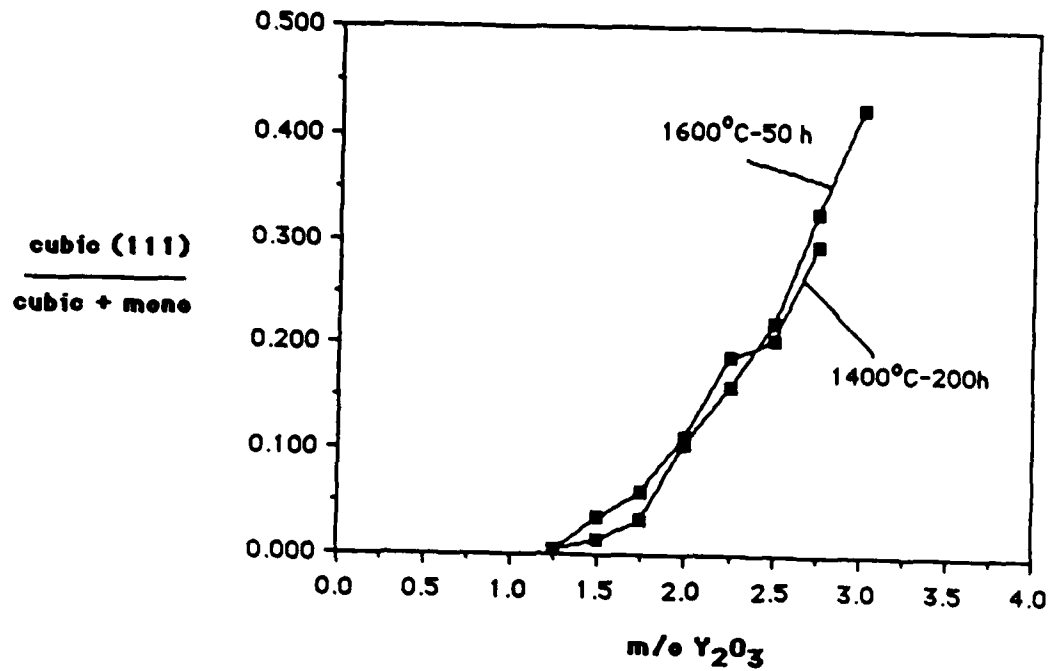Figure 1 Schematic of the ZrO_2-rich portion of the ZrO_2-Y_2O_3 binary system.

Figure 2 Cubic phase content vs composition after 50 h and 200 h heat treatments at 1600 °C and 1400 °C, respectively.

Figure 3 Yttrium content of individual grains for a composition containi g 2.25 m/o Y_2O_3 after heat treatment at 1400 °C for 1 and 50 h.

Figure 4 Grain size vs Y_2O_3 content for different heat treatment periods at 1400 °C and 1600 °C

Figure 5 Grain size vs heat treatment period at 1400 °C for sintered material containing 3 m/o Y_2O_3 . Arrows indicate first observation of cubic and monoclinic structures by XRD of sintered material.

Figure 6 Critical stress intensity factor vs heat treatment period at 1400 °C for sintered material.

Figure 7 Raman microprobe results of calibrated volume fraction of tetragonal ZrO_2 vs perpendicular distance from edge of vickers indentation after different heat treatments of sintered material.

Figure 8 Schematic of free energy vs composition function for tetragonal and cubic ZrO_2 structures at heat treatment temperature.

Figure 1

Figure 2 Cubic phase content vs composition after 50 h and 200 h heat treatments at 1600 °C and 1400 °C, respectively.
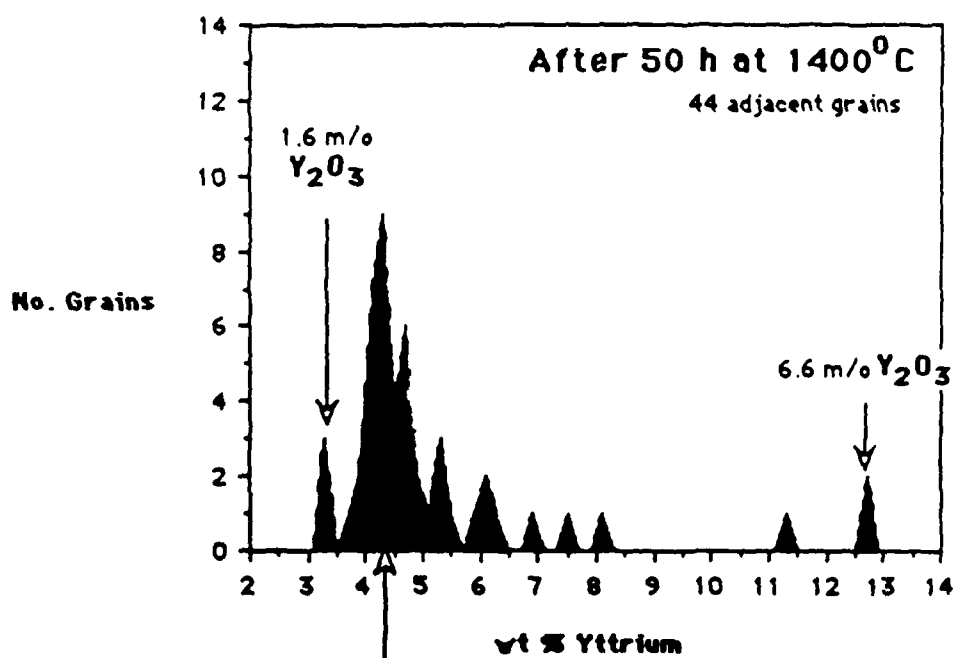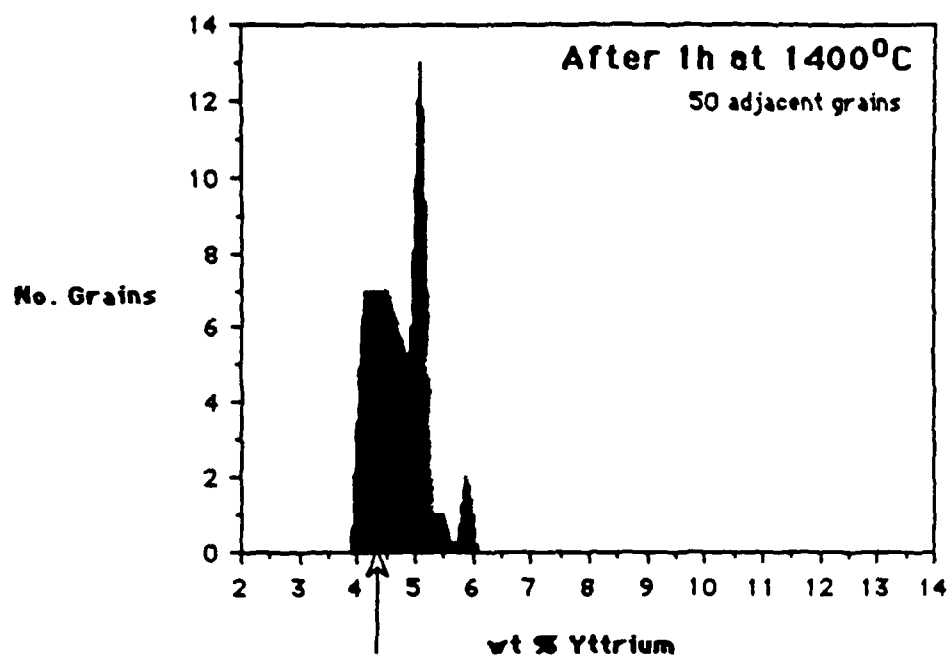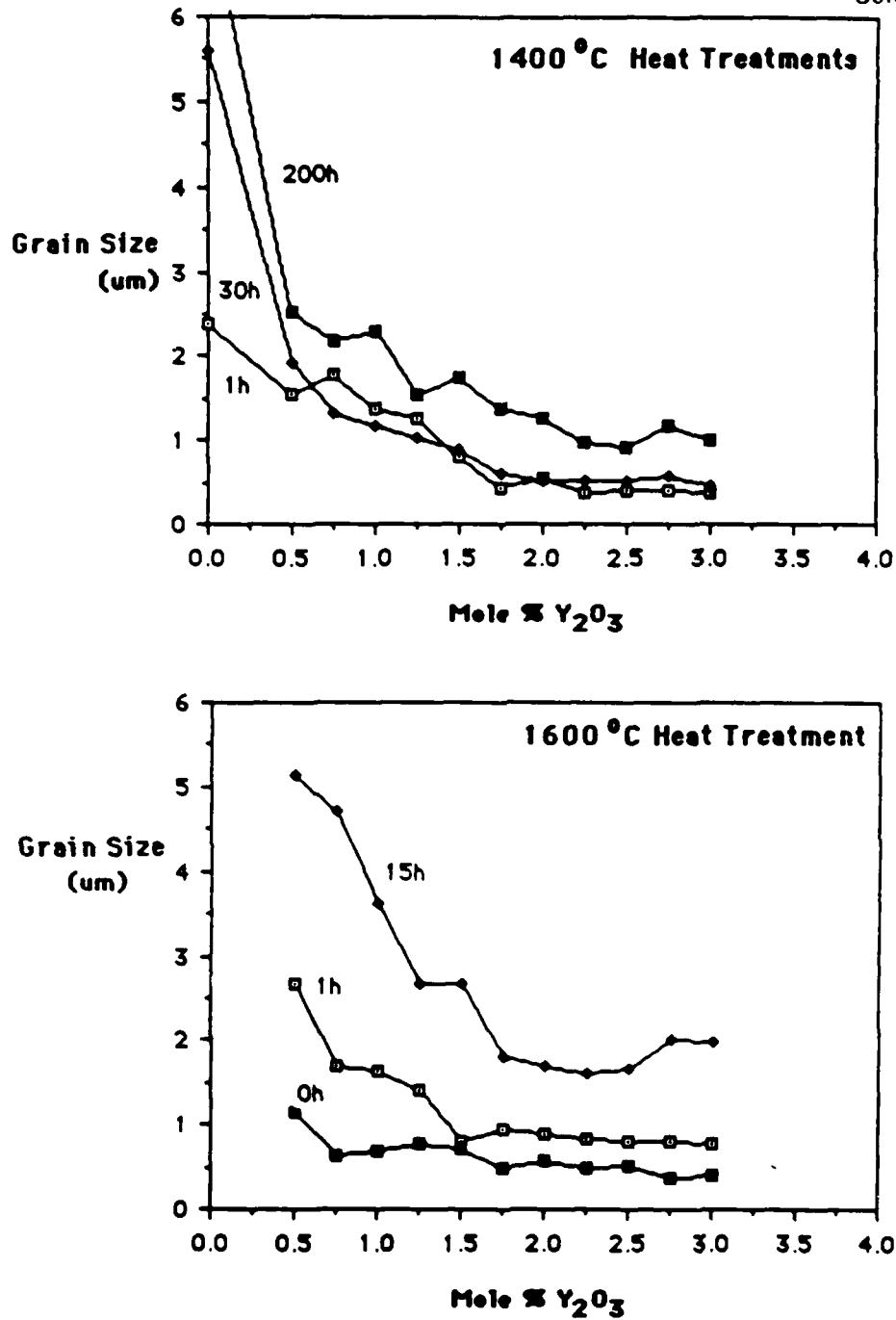
Figure 3 Yttrium content of individual grains for a composition containing 2.25 m/o Y_2O_3 after heat treatment at 1400 °C for 1 and 50 h.

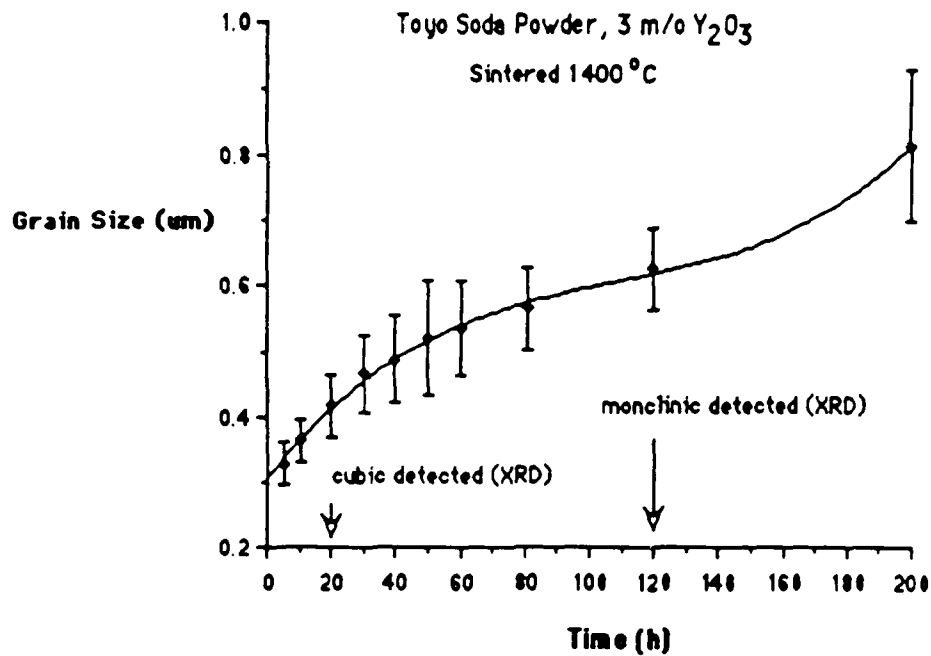Figure 4 Grain size vs Y_2O_3 content for different heat treatment periods at 1400 °C and 1600 °C

Figure 5 Grain size vs heat treatment period at 1400 °C for sintered material containing 3 m/o Y_2O_3 . Arrows indicate first observation of cubic and monoclinic structures by XRD of sintered material.
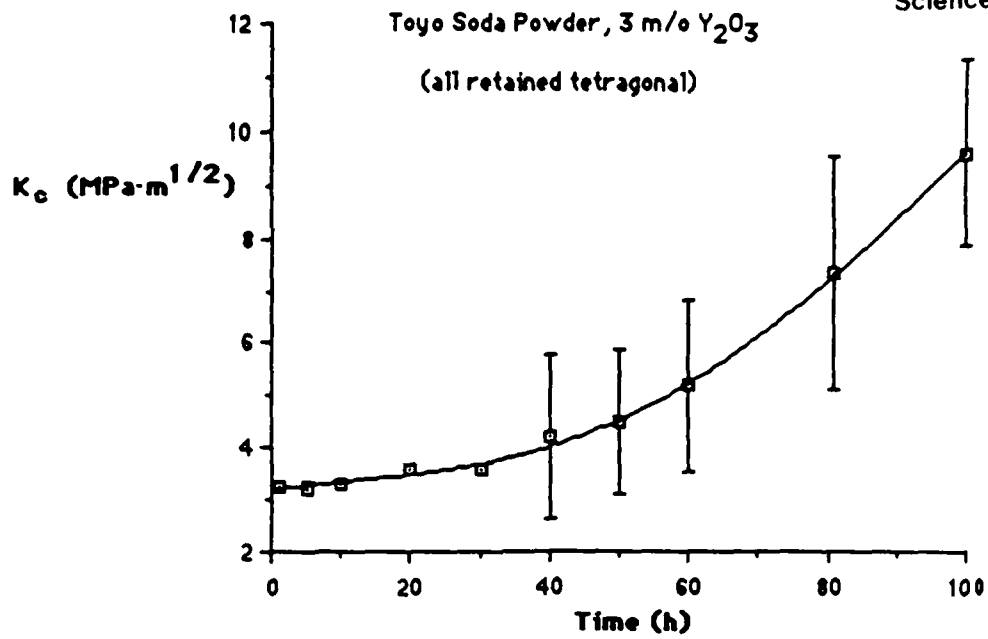
118

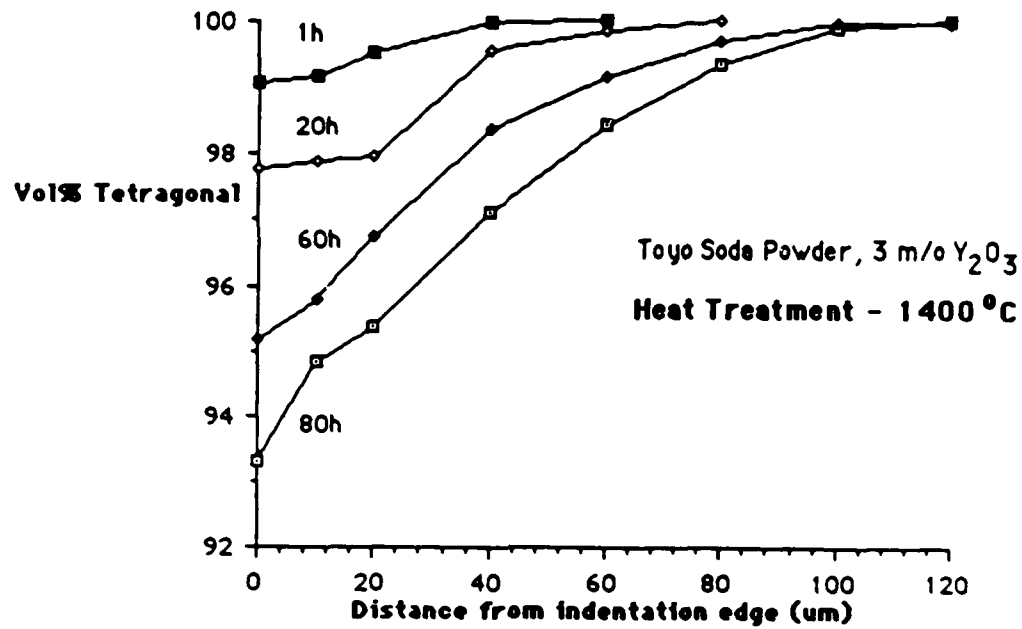Figure 6 Critical stress intensity factor vs heat treatment period at 1400 °C for sintered material.

Figure 7 Raman microprobe results of calibrated volume fraction of tetragonal ZrO_2 vs perpendicular distance from edge of vickers indentation after different heat treatments of sintered material.
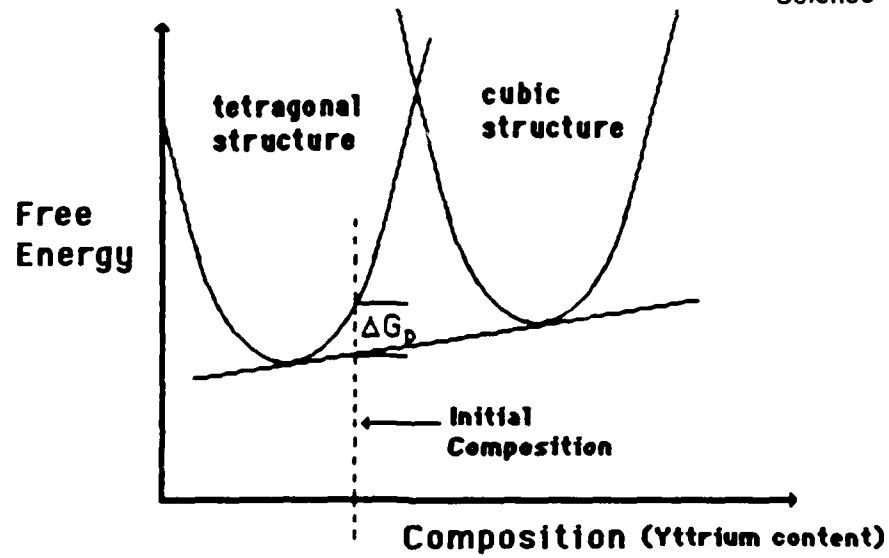
Figure 8 Schematic of free energy vs composition function for tetragonal and cubic ZrO_2 structures at heat treatment temperature.

END

DATE

FILMED

DTIC

4/88